Fundamentals of XAFS

Matthew Newville
Consortium for Advanced Radiation Sources
University of Chicago, Chicago, IL

Contents

Chapter 1

Introduction

X-ray absorption fine structure (XAFS) refers to the details of how x-rays are absorbed by an atom at energies near and above the core-level binding energies of that atom. Specifically, XAFS is the modulation of an atom's x-ray absorption probability due to the chemical and physical state of the atom. XAFS spectra are especially sensitive to the formal oxidation state, coordination chemistry, and the distances, coordination number and species of the atoms immediately surrounding the selected element. Because of this dependence, XAFS provides a practical, and relatively simple, way to determine the chemical state and local atomic structure for a selected atomic species. XAFS can be used in a variety of systems and bulk physical environment. XAFS is routinely used in a wide range of scientific fields, including biology, environmental science, catalysts research, and material science.

Since XAFS is an atomic probe, it places few constraints on the samples that can be studied. All atoms have core level electrons, and XAFS spectra can be measured for essentially every element on the periodic table. Importantly, crystallinity is not required for XAFS measurements, making it one of the few structural probes available for noncrystalline and highly disordered materials, including solutions. Because x-rays are fairly penetrating in matter, XAFS is not inherently surface-sensitive, though special measurement techniques can be applied to enhance its surface sensitivity. In many cases, XAFS measurements can be made on elements of minority and even trace abundance, giving a unique and direct measurement of chemical and physical state of dilute species in a variety of systems.

X-ray absorption measurements are relatively straightforward, provided one has an intense and energy-tunable source of x-rays. In practice, this usually means the use of synchrotrons, and the history and development of XAFS closely parallels that of synchrotron radiation. Many experimental techniques and sample conditions are available for XAFS, including such possibilities as very fast measurements of *in situ* chemical processes, high spatial resolution, and extreme conditions of temperature and pressure. Since the characteristics of synchrotron sources and experimental station dictate what energy ranges, beam sizes, and intensities are available, this often puts practical experimental limits on the XAFS measurements that can be done even if there are few inherent limits on XAFS.

Though the measurements can be simple, a complete understanding of XAFS in-

volves a wonderful mixture of modern physics and chemistry and a complete mastery of the data analysis can be somewhat challenging. Though the basic phenomena is well-understood, an accurate theoretical treatment is fairly involved and, in some respects still an area of active research. The interpretation and analysis of XAFS is not always straightforward, though significant progress has been made in both the theoretical and analytical tools for XAFS in the past decade or so. Accurate and precise interpretation of XAFS spectra is routine, if not always trivial for novice experimentalists.

The x-ray absorption spectrum is typically divided into two regimes: x-ray absorption near-edge spectroscopy (XANES) and extended x-ray absorption fine-structure spectroscopy (EXAFS). Though the two have the same physical origin, this distinction is convenient for the interpretation. XANES is strongly sensitive to formal oxidation state and coordination chemistry (e.g., octahedral, tetrahedral coordination) of the absorbing atom, while the EXAFS is used to determine the distances, coordination number, and species of the neighbors of the absorbing atom.

In this work, the origins and interpretations of XAFS will be introduced, with a hope of aiding the reader to be able to make high-quality XAFS measurements as well as process and analyze the data. It is not likely that one could become an expert simply by reading this introduction to XAFS, but it should provide a starting place for a new practitioner of XAFS. The reader is not expected to have previous experience with XAFS or or x-ray measurements, but some familiarity with advanced undergraduate-level chemistry or physics and a general knowledge of experimental practices and data interpretation will be helpful.

Chapter 2

X-Ray Absorption and Fluorescence

X-rays are light with energies ranging from ~ 500 eV to 500 keV, or wavelengths from ~ 25Å to 0.25Å. At this energy regime, light is absorbed by all matter through the *photo-electric effect*. In this process, an x-ray photon is absorbed by an electron in a tightly bound quantum core level (such as the 1s or 2p level) of an atom (Fig 2.1).

In order for a particular electronic core level to participate in the absorption, the binding energy of this core level must be less than the energy of the incident x-ray. If the binding energy is *greater than* the energy of the x-ray, the bound electron will not be perturbed from the dell-defined quantum state and will not absorb the x-ray. If the binding energy of the electron is *less than* that of the x-ray, the electron may be removed from its quantum level. In this case, the x-ray is destroyed (i.e., absorbed) and any energy in excess of the electronic binding energy is given to a photo-electron that is ejected from the atom. This process has been well understood for nearly a century (Einstein received the Nobel Prize for describing this effect). The full implications of this process when applied to molecules, liquids, and solids will give rise to XAFS.

When discussing x-ray absorption, we are primarily concerned with the *absorption coefficient*, μ which gives the probability that x-rays will be absorbed according to Beer's Law:

$$I = I_0 e^{-\mu t} \tag{2.1}$$

where I_0 is the x-ray intensity incident on a sample, t is the sample thickness, and I is the intensity transmitted through the sample, as shown in Fig 2.2. For x-rays, as for all light, the x-ray intensity is proportional to the number of x-ray photons.

At most x-ray energies, the absorption coefficient μ is a smooth function of energy, with a value that depends on the sample density ρ, the atomic number Z, atomic mass A, and the x-ray energy E roughly as

$$\mu \approx \frac{\rho Z^4}{AE^3}. \tag{2.2}$$

The strong dependence of μ on both Z and E is a fundamental property of x-rays, and is the key to why x-ray absorption is useful for medical and other imaging techniques, including x-ray computed tomography. Due to the $Z4$ dependence, the absorption coefficient for O, Ca, Fe, and Pb are very different – spanning several orders of magnitude – so that good contrast between different materials can be achieved for
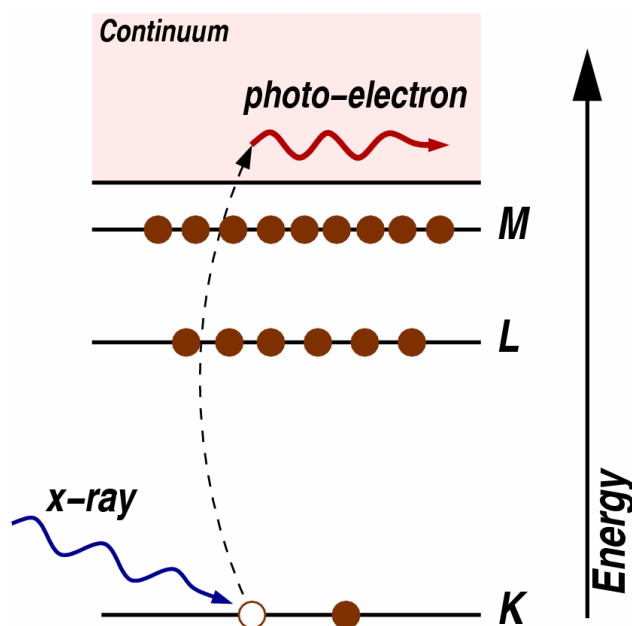
Figure 2.1: The photoelectric effect, in which an x-ray is absorbed and a core-level electron is promoted out of the atom.

nearly any sample thickness and concentrations by adjusting the x-ray energy. Fig 2.3 shows the energy-dependence of μ/ρ for O, Fe, Cd, and Pb.

When the incident x-ray has an energy equal to that of the binding energy of a core-level electron, there is a sharp rise in absorption: an *absorption edge* corresponding to the promotion of this core level to the continuum. For XAFS, we are concerned with the intensity of μ as a function of energy, near and at energies just above these absorption edges. An XAFS measurement is simply a measure of the energy dependence of μ at and above the binding energy of a known core level of a known atomic species. Since every atom has core-level electrons with well-defined binding energies, we can select the element to probe by tuning the x-ray energy to an appropriate absorption edge. These

Figure 2.2: x-ray absorption measurements: An incident beam of monochromatic x-rays of intensity I_0 passes through a sample of thickness t, and the transmitted beam has intensity I.

absorption edge energies are well-known (usually to within a tenth of percent), and tabulated. The edge energies vary with atomic number approximately as Z^2, but both K and L levels can be used in the hard x-ray regime (in addition, M edges can be for heavy elements in the soft x-ray regime), which allows most elements to be probed by XAFS with x-ray energies between 5 and 35 keV, as shown in Fig 2.4. Because the element of interest is chosen in the experiment, XAFS is *element-specific*.
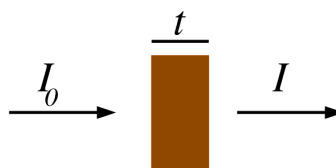
Following an absorption event, the atom is said to be in an *excited state*, with one of the core electron levels left empty (a so-called *core hole*), and a *photo-electron*. The ex-
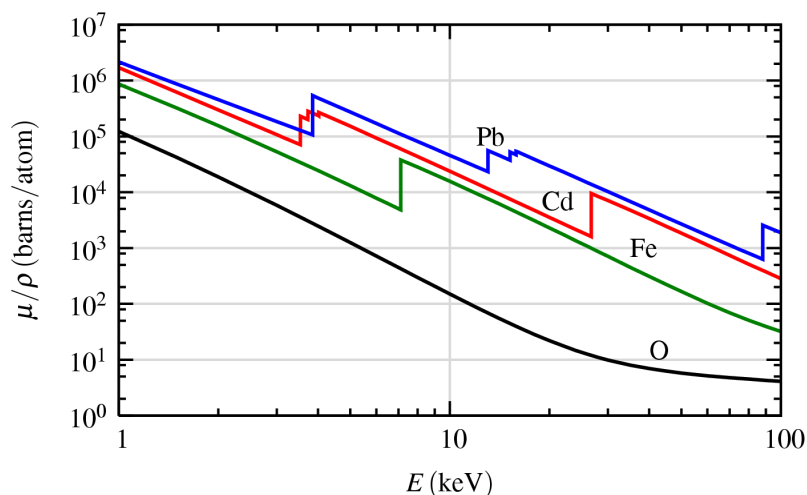
Figure 2.3: The absorption cross-section μ/ρ for several elements over the x-ray energy range of 1 to 100 keV. Notice that there are at least 5 orders of magnitude in variation in μ/ρ, and that in addition to the strong energy dependence, there are also sharp rises corresponding to the core-level binding energies of the atoms.

cited state will eventually decay typically within a few femtoseconds of the absorption event. Though this decay does not affect the x-ray absorption process, it is important for the discussion below.

There are two main mechanisms for the decay of the excited atomic state following an x-ray absorption event. The first of these is x-ray fluorescence (Fig 2.5), in which a higher energy electron core-level electron fills the deeper core hole, ejecting an x-ray of well-defined energy. The fluorescence energies emitted in this way are characteristic of the atom, and can be used to identify the atoms in a system, and to quantify their concentrations. For example, an L shell electron dropping into the K level gives the K_α fluorescence line.

The second process for de-excitation of the core hole is the Auger Effect, in which an electron drops from a higher electron level and a second electron is emitted into the continuum (and possibly even out of the sample). In the hard x-ray regime ($> 2\,\mathrm{keV}$), x-ray fluorescence is more likely to occur than Auger emission, but for lower energy x-ray absorption, Auger processes dominate. Either of these processes can be used to measure the absorption coefficient μ, though the use of fluorescence is somewhat more common.

XAFS can be measured either in transmission or fluorescence geometries as shown in Fig 2.2. (The geometry for Auger measurements is typically the same as for fluorescence). We will return to the details of the measurements later. For now it is enough to say that we can measure the energy dependence of the absorption coefficient $\mu(E)$ either in transmission as
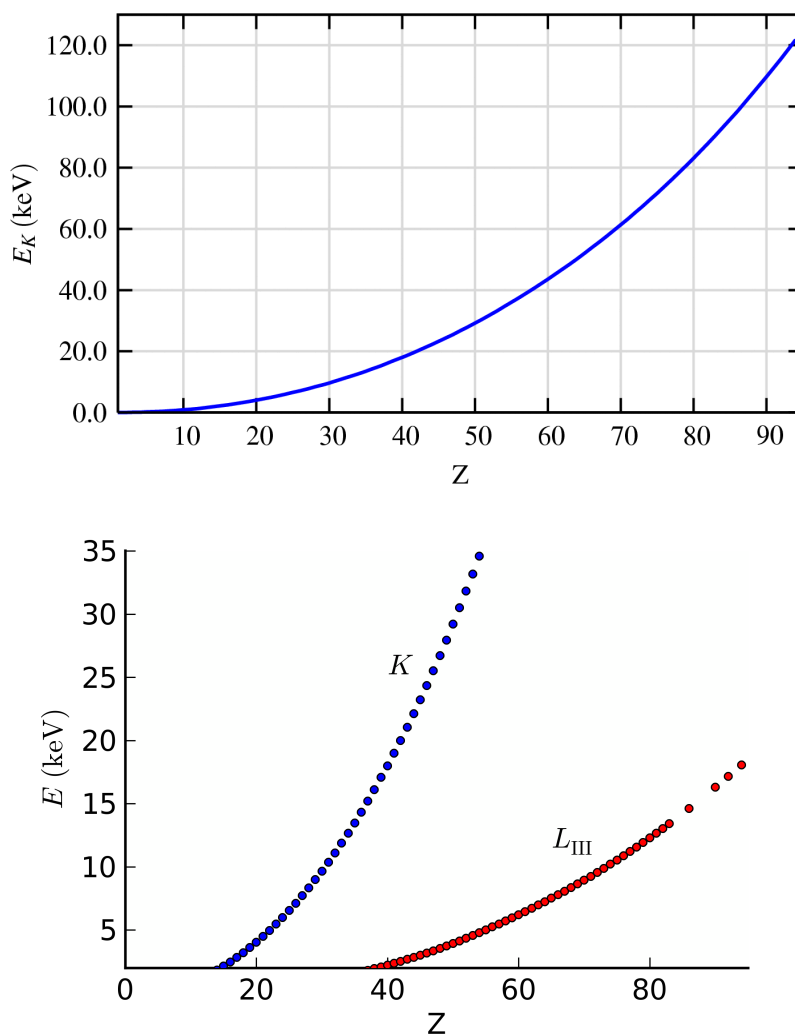
$$\mu(E) = \log(I_0/I) \tag{2.3}$$

Figure 2.4: The energy of the x-ray K and L_{III} absorption edges as a function of atomic number Z.

or in x-ray fluorescence (or Auger emission) as

$$\mu(E) \propto I_f/I_0 \tag{2.4}$$

where I_f is the monitored intensity of a fluorescence line (or, again, electron emission) associated with the absorption process.

A typical XAFS spectrum (measured in the transmission geometry for a powder of FeO) is shown in Fig 2.6. The sharp rise in $\mu(E)$ due to the Fe 1s electron level (at 7112 eV) is clearly visible in the spectra, as are the oscillations in $\mu(E)$ that are the XAFS. As mentioned in the introduction, the XAFS is generally thought of in two distinct portions: the near-edge spectra (XANES) – typically within 30eV of the main absorption edge, and the extended fine-structure (EXAFS). As we shall, the basic physical description of these two regimes is the same, but some important approximations
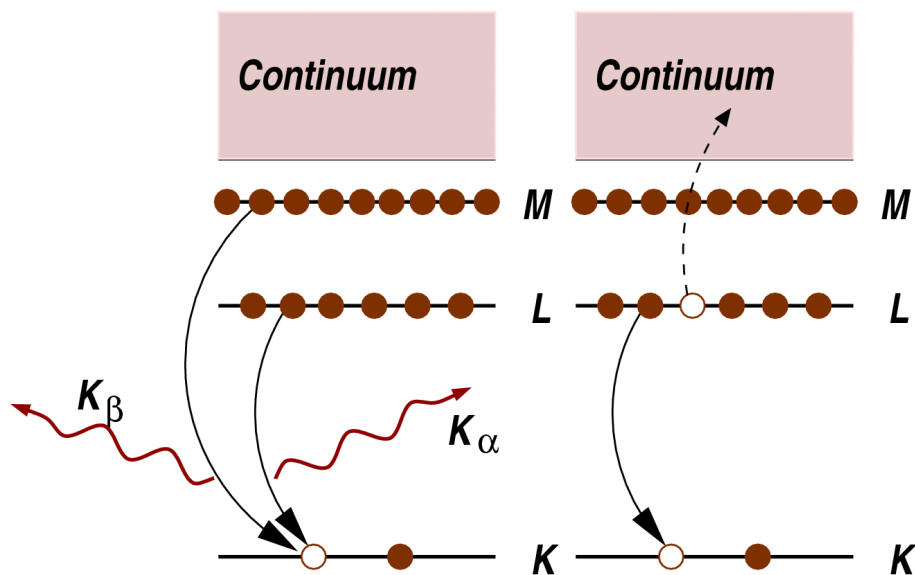
Figure 2.5: Decay of the excited state: x-ray fluorescence (left) and the Auger effect (right). In both cases, the probability of emission (x-ray or electron) is directly proportional to the absorption probability.

and limits allow us to interpret the extended spectra in a more quantitative way than is currently possible for the near-edge spectra.

For the EXAFS, we are interested in the oscillations well above the absorption edge, and define the EXAFS fine-structure function $\chi(E)$, as

$$\chi(E) = \frac{\mu(E) - \mu_0(E)}{\Delta\mu_0(E)} \qquad (2.5)$$

where $\mu(E)$ is the measured absorption coefficient, $\mu_0(E)$ is a smooth background function representing the absorption of an isolated atom, and $\Delta\mu_0$ is the measured jump in the absorption $\mu(E)$ at the threshold energy E_0 (Fig 2.6 bottom).

As we will see below, EXAFS is best understood in terms of the wave behavior of the photo-electron created in the absorption process. Because of this, it is common to convert the x-ray energy to k, the wave number of the photo-electron, which has dimensions of 1/distance and is defined as

$$k = \sqrt{\frac{2m(E - E_0)}{\hbar^2}} \qquad (2.6)$$

where E_0 is the absorption edge energy and m is the electron mass. The primary quantity for EXAFS is then $\chi(k)$, the oscillations as a function of photo-electron wave number, and $\chi(k)$ is often referred to simply as "the EXAFS". In this way, the EXAFS extracted from the Fe K-edge for FeO is shown in Fig 2.7 (top). As you can see, the EXAFS is oscillatory and decays quickly with k. To emphasize the oscillations, $\chi(k)$ is often multiplied by a power of k typically k^2 or k^3, as shown in Fig 2.7 (bottom).
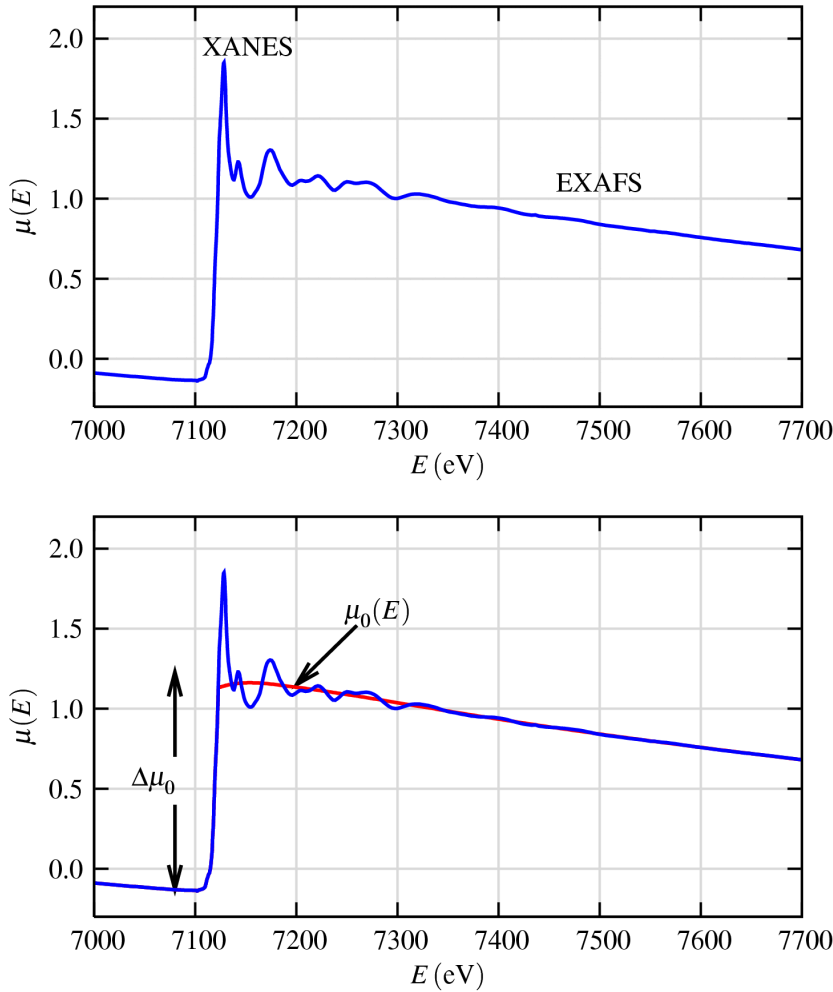
Figure 2.6: XAFS $\mu(E)$ for FeO. On top, the measured XAFS spectrum is shown with the XANES and EXAFS regions identified. On the bottom, $\mu(E)$ is shown with smooth background function $\mu_0(E)$ and the edge-step $\Delta\mu_0(E_0)$.

The different frequencies apparent in the oscillations in $\chi(k)$ correspond to different near-neighbor coordination shells which can be described and modeled according to the *EXAFS Equation*,

$$\chi(k) = \sum_j \frac{N_j f_j(k) e^{-2k^2 \sigma_j^2}}{k R_j^2} \sin[2k R_j + \delta_j(k)] \tag{2.7}$$

where $f(k)$ and $\delta(k)$ are scattering properties of the atoms neighboring the excited atom, N is the number of neighboring atoms, R is the distance to the neighboring atom, and σ^2 is the disorder in the neighbor distance. Though somewhat complicated, the EXAFS equation allows us to determine N, R, and σ^2 knowing the scattering amplitude $f(k)$ and phase-shift $\delta(k)$. Furthermore, since these scattering factors depend
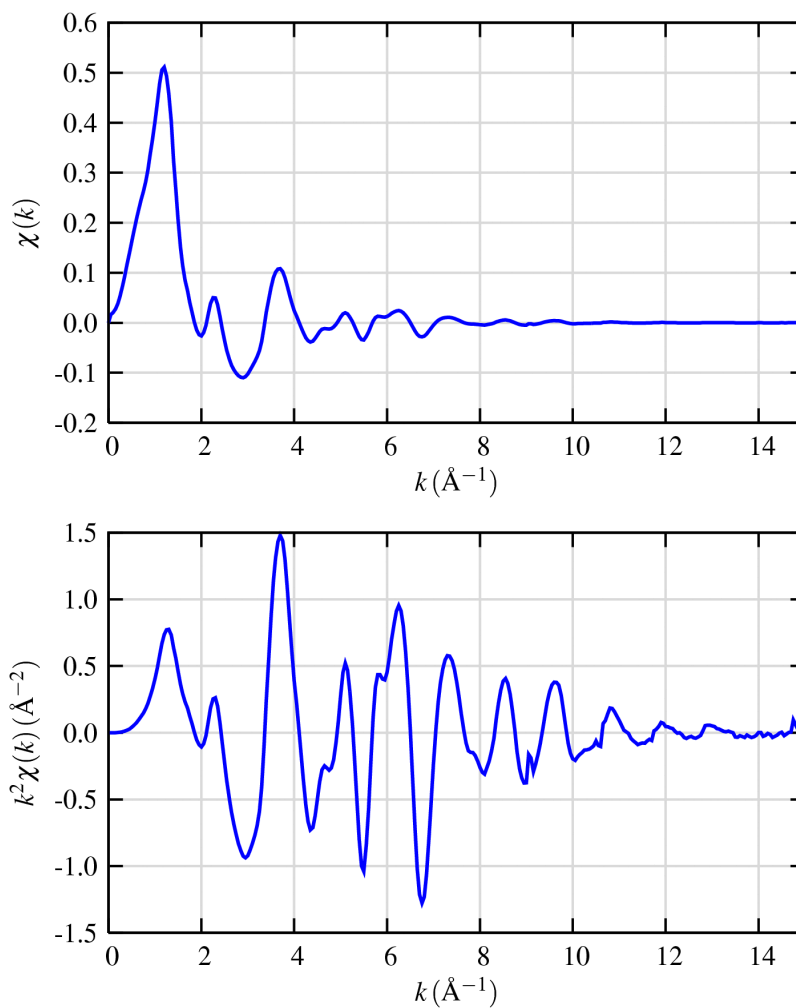
Figure 2.7: Isolated EXAFS $\chi(k)$ for FeO (top), and the k-weighted XAFS, $k^2\chi(k)$ (bottom).

on the Z of the neighboring atom, EXAFS is also sensitive to the atomic species of the neighboring atom.

Chapter 3

A Simple Theoretical Description of XAFS

In this section, a simple physical description of the XAFS process and the origin of the EXAFS Equation will be given. As described above, we start with the photoelectric effect, now shown in Fig 3.1, in which an x-ray is absorbed by a core-level with binding energy, and a photo-electron with wave number k is created and propagates away from the atom.

An important point for the discussion here is that the absorption due to a given core-level relies on there being an *available state* for the photo-electron: a quantum state at exactly the right energy, and also the right angular momentum state. If there is no available state, there will be no absorption from that core level. For example, at energies below the $1s$ binding energy, a $1s$ electron could only be promoted to a p valence level below the binding energy (or Fermi level). Since all the available valence levels are filled by the valence electrons, there is no state for the $1s$ electron to fill, and so there is no absorption from that core-level. There is still some absorption, of course, because higher level electrons can be promoted into the continuum.

When a neighboring atom is included in the picture (Fig 3.2), the photo-electron can scatter from the electrons of this neighboring atom, and the scattered photo-electron can return to the absorbing atom. Since the absorption coefficient depends on whether there is an available electronic state (that is whether there is an electron at the location of the atom and at the appropriate energy and momentum), the presence of the photo-electron scattered back from the neighboring atom will alter the absorption coefficient: This is the origin of XAFS.

We'll now develop the XAFS equation using a slightly more formal description of this simple physical picture. Since x-ray absorption is a *transition* between two quantum states (from an initial state with an x-ray, a core electron, and no photo-electron to a final state with no x-ray, a core hole, and a photo-electron), we describe $\mu(E)$ with Fermi's Golden Rule:

$$\mu(E) \propto |\langle i|\mathcal{H}|f\rangle|^2 \tag{3.1}$$

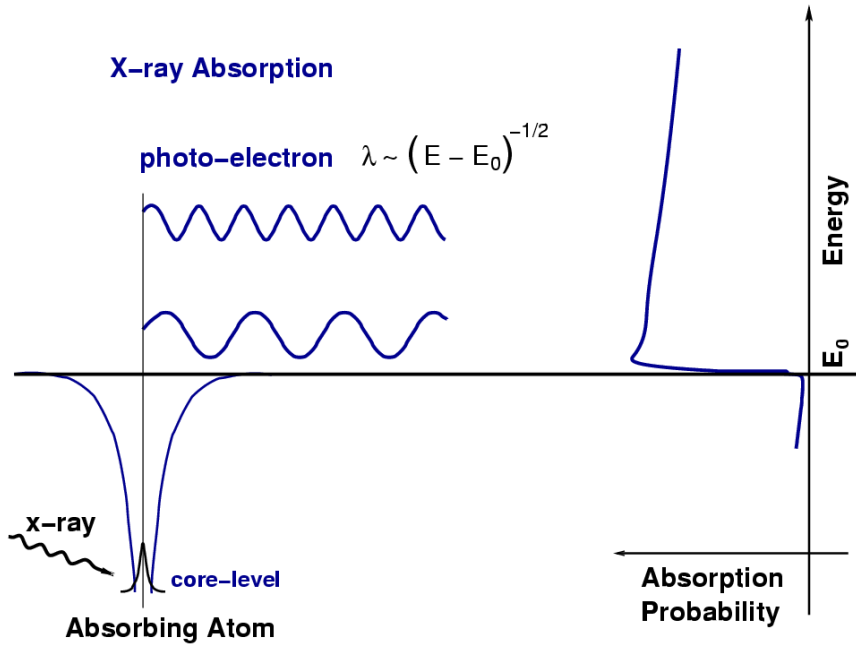where $\langle i|$ represents the initial state (an x-ray, a core electron, and no photo-electron),

Figure 3.1: Cartoon of x-ray absorption through the photoelectric process. When an x-ray has the energy of a tightly bound core electron level, E_0, the probability of absorption has a sharp rise. In the absorption process, the tightly bound core-level is destroyed, and a photo-electron is created. The photo-electron travels as a wave with wave number proportional to $\sqrt{(E - E_0)}$.

$|f\rangle$ is the final state (no x-ray, a core-hole, and a photo-electron), and $\mathcal{H}$ is the inter-action term (which we'll come back to shortly). Since the core-level electron is very tightly bound to the absorbing atom, the initial state will not be altered by the presence of the neighboring atom. The final state, on the other hand, will be affected by the neighboring atom because the photo-electron will be able to see it. If we expand $|f\rangle$ into two pieces, one that is the "bare atom" portion ($|f_0\rangle$), and one that is the effect of the neighboring atom ($|\Delta f\rangle$) as

$$|f\rangle = |f_0\rangle + |\Delta f\rangle, \tag{3.2}$$

we can expand Eq. 3.1 to

$$\mu(E) \propto |\langle i|\mathcal{H}|f_0\rangle|^2 \big[1 + \langle i|\mathcal{H}|\Delta f\rangle \frac{\langle f_0|\mathcal{H}|i\rangle^*}{|\langle i|\mathcal{H}|f_0\rangle|^2} + C.C\big] \tag{3.3}$$

where C.C. means complex conjugate. We've arranged the terms here so that this ex-pression resembles our previous relationship between $\mu(E)$ and $\chi(E)$,

$$\mu(E) = \mu_0(E)[1 + \chi(E)]. \tag{3.4}$$

We can now assign $\mu_0 = |\langle i|\mathcal{H}|f_0\rangle|^2$ as the "bare atom absorption", which depends only on the absorbing atom – as if the neighboring atom wasn't even there. We can also
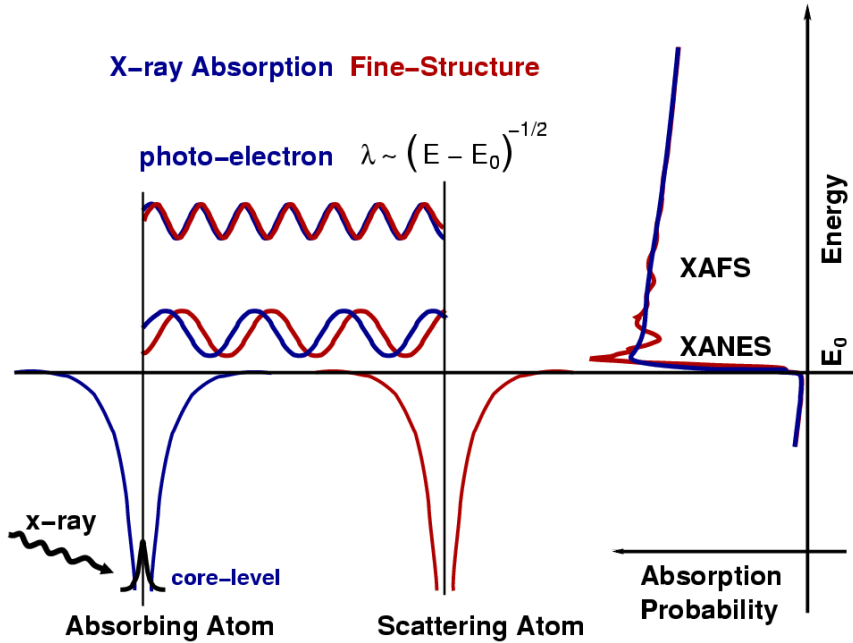
Figure 3.2: XAFS occurs because the photo-electron can scatter from a neighboring atom. The scattered photo-electron can return to the absorbing atom, modulating the amplitude of the photo-electron wave-function at the absorbing atom. This in turn modulates the absorption coefficient $\mu(E)$, causing the EXAFS.

see that fine-structure χ can be written as

$$\chi(E) \propto \langle i | \mathcal{H} | \Delta f \rangle. \tag{3.5}$$

We can work this out (at least roughly) as an integral equation fairly easily. The interaction term $\mathcal{H}$ is probably the most mysterious part – it represents the process of changing between two energy, momentum states. If you're familiar with quantum radiation theory, the interaction term needed is the $\mathbf{p} \cdot \mathbf{A}$ term, where $\mathbf{A}$ is the quantized vector potential (the $\mathbf{A} \cdot \mathbf{A}$ term, but this does not contribute to absorption). For the purposes here, this reduces to a term that is proportional to e^{ikr}. The initial state is a tightly bound core-level, which we can approximate by delta function (a 1s level for atomic number Z extends to around a_0/Z, where a_0 is the Bohr radius of $\sim 0.529\,\text{Å}$). The change in final state is just the wave-function of the scattered photo-electron, $\psi_{\text{scatt}}(r)$. Putting all these terms together, we get a simple expression for the EXAFS:

$$\chi(E) \propto \int dr \delta(r) e^{ikr} \psi_{\text{scatt}}(r) = \psi_{\text{scatt}}(0). \tag{3.6}$$

In words, this simply states the physical picture shown in Fig 3.2:

> **The EXAFS $\chi(E)$ is proportional to the amplitude of the scattered photo-electron at the absorbing atom.**

We can further evaluate the amplitude of the scattered photo-electron at the absorbing atom, to get the EXAFS equation. Again, using the simple physical picture from Fig 3.2, we can describe the outgoing photo-electron wave-function $\psi(k, r)$ traveling as a spherical wave,

$$\psi(k, r) = \frac{e^{ikr}}{kr}, \tag{3.7}$$

traveling a distance R to the neighboring atom, then scattering from a neighbor atom, and traveling as a spherical wave a distance R back to the absorbing atom. We simply multiply all these factors together to get

$$\chi(k) \propto \psi_{\text{scatt}}(k, r = 0) = \frac{e^{ikR}}{kR} \left[2kf(k)e^{i\delta(k)} \right] \frac{e^{ikR}}{kR} + C.C. \tag{3.8}$$

where $f(k)$ and $\delta(k)$ are scattering properties of the neighboring atom. As mentioned before, these scattering factors depend on the Z of the neighboring atom, as shown in Fig 3.3. These scattering factors make EXAFS sensitive to the atomic species of the neighboring atom. Combining these terms in and including the complex conjugate to make sure we end up with a real function, we get

$$\chi(k) = \frac{f(k)}{kR^2} \sin[2kR + \delta(k)] \tag{3.9}$$

which looks much like the XAFS equation above. The treatment here was for one pair of absorbing atom and scattering atom, but for a real measurement we'll average over millions of atom pairs. Even for neighboring atoms of the same type, the thermal and static disorder in the bond distances will give a range of distances that will affect the XAFS. As a first approximation, this disorder will change the XAFS equation to

$$\chi(k) = \frac{Ne^{-2k^2\sigma^2}f(k)}{kR^2} \sin[2kR + \delta(k)] \tag{3.10}$$

where N is the coordination number and σ^2 is the mean-square-displacement in the bond distance R. More sophisticated and general approaches to thermal and static disorder, including non-Gaussian distributions of atomic distributions are possible (and routinely used in analysis), but are beyond the scope of the treatment here.

Of course, real systems usually have more that one type of neighboring atom around a particular absorbing atom. This is easily accommodated in the XAFS formalism, as the measured XAFS will simply be a sum of the contributions from each scattering atom type (or *coordination shell*, as it is often called – the terms *coordination sphere* and *scattering path* are also used),

$$\chi(k) = \sum_j \frac{N_j e^{-2k^2\sigma_j^2} f_j(k)}{kR_j^2} \sin[2kR_j + \delta_j(k)] \tag{3.11}$$

where j represents the individual coordination shell of identical atoms at approximately the same distance from the central atom. In principle there could be many such shells, but as shells of similar Z become close enough (i.e., within a 0.05Åof each other), they become difficult to distinguish from one another.
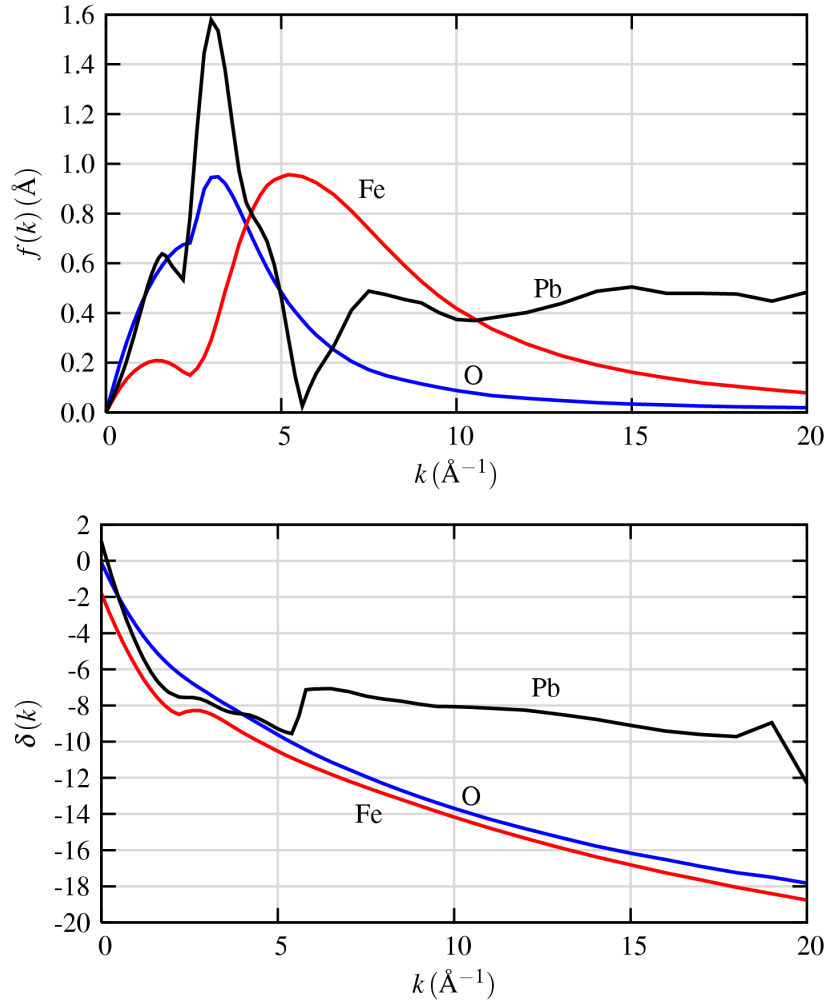
Figure 3.3: Functional forms for $f(k)$ (top) and $\delta(k)$ (bottom) for O, Fe, and Pb showing the dependence of these terms on atomic number Z. The variations in functional form allow Z to be determined (± 5 or so) from analysis of the EXAFS.

We now return to correct one of the most important approximations we made above. When we asserted that the outgoing photo-electron went out as a spherical wave in Eq. 3.7, we neglected the fact that the photo-electron can also scatter *inelastically* from other sources – other conduction electrons, phonons, and so on. In order to participate in the XAFS, the photo-electron has to scatter from the neighboring atom and return to the absorbing atom *elastically* (i.e., at the same energy) as the outgoing photo-electron. In addition, the photo-electron has to make it back to the absorbing atom before the excited state decays (i.e., before the core-hole is filled). To account for both the inelastic scattering and the *core-hole lifetime*, we use a damped spherical wave

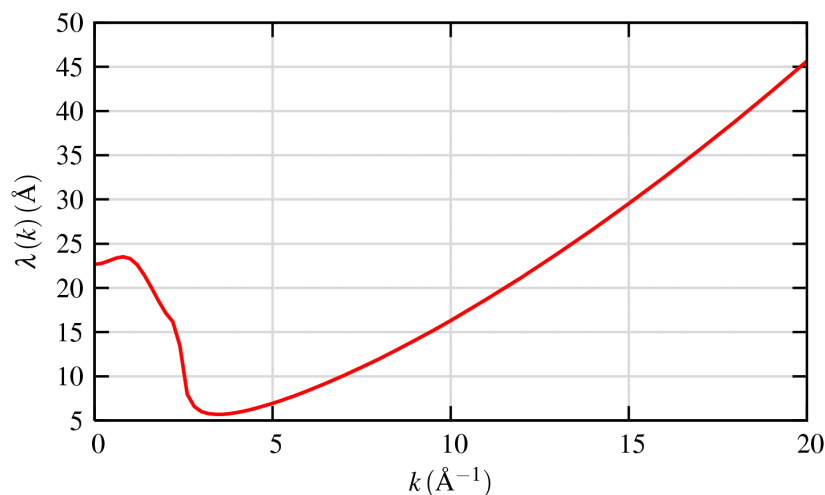$$\psi(k, r) = \frac{e^{ikr}e^{-2r/\lambda(k)}}{kr},$$
(3.12)

Figure 3.4: The photo-electron mean-free-path for XAFS $\lambda(k)$, representing how far the photo-electron can travel and still participate in the XAFS. This term includes both the inelastic scattering of the photo-electron, and the effect of the finite lifetime of the core-hole.

as the photo-electron wave-function where λ is the mean-free-path of the photo-electron (that is, how far it typically travels before scattering inelastically and before the core-hole is filled). The mean-free-path is typically 5 to 30Å and has a significant but fairly universal dependence on k, shown in Fig 3.4. Including the $\lambda(k)$, the EXAFS equation becomes

$$\chi(k) = \sum_j \frac{N_j e^{-2k^2\sigma_j^2} e^{-2R_j/\lambda(k)} f_j(k)}{k R_j^2} \ \sin[2kR_j + \delta_j(k)] \qquad (3.13)$$

From this equation, we can draw a few physical conclusions about XAFS. First, because of the $\lambda(k)$ term and the R^{-2} term, XAFS is seen to be an inherently *local probe*, not able to see much further than 5 or so Angstroms from the absorbing atom. Second, the XAFS oscillations will consist of different frequencies that correspond to the different distances for each coordination shell. This will lead us to use Fourier transforms in the analysis. Finally, in order to extract the distances and coordination numbers, we need to have accurate values for the scattering amplitude and phase-shifts $f(k)$ and $\delta(k)$.

This last point here – the need for accurate scattering amplitude and phase-shifts – has been a crucial issue in the field of EXAFS. Though early attempts to calculate the terms were qualitatively successful and instructive, they were generally not accurate enough to be used in analysis. In the earliest EXAFS analyses, these factors could only be determined accurately from experimental spectra in which the near-neighbor distances and species were known (generally from measurements of crystals with well-known structures). Such experimental standards can be quite accurate, but are generally restricted to first neighbor shell. Up until the early 1990's their use was quite common. In the past decade or so, calculations of $f(k)$ and $\delta(k)$ have become more accurate and readily available, and use of experimental standards in EXAFS analysis is now some-

what rare. Calculated scattering factors such as those from the programs FEFF, GNXAS, and EXCURVE are not without problems, but they have been shown numerous times to be accurate enough to be used in real analysis, and in some cases are more accurate than experimentally derived scattering factors. In addition, the calculated factors are not restricted to the first shell, can account for multiple-scattering of the photo-electron. In section 6, we'll use calculations of $f(k)$ and $\delta(k)$ from FEFF, though we won't go into details of the mechanics of how FEFF (or any other program) is run.

We have seen that the physical description of x-ray absorption as creation of a photo-electron into an available electronic level, and the realization that this photo-electron will scatter from neighboring atoms leads to a simple explanation of the modulations in the x-ray absorption coefficient above an absorption edge. Furthermore, we've used this simple physical picture to develop the XAFS equation that we can use in the quantitative analysis of XAFS spectra.

Chapter 4

XAFS Measurements: Transmission and Fluorescence

XAFS requires a very good measure of $\mu(E)$. Since the XAFS is a small part of the total absorption, a fairly precise and accurate measurement of $\mu(E)$ – typically to 10^{-3} – is required. Errors in the measurement of $\mu(E)$ can degrade or even destroy the XAFS. Fortunately, if care is taken, it is usually not too difficult to get good measurements.

Following the picture of the experimental layout in Fig 2.2, the main experimental challenges are 1) getting an x-ray source that can be reliably and precisely tuned to select a single x-ray energy, and 2) high-quality detectors of x-ray intensity. For most experiments, the tunable x-ray source is a synchrotron, which provides a full range of x-ray wavelengths, and a particular energy is selected with a double crystal monochromator made from silicon based on Bragg diffraction. A double crystal monochromator consists of a first crystal that is rotated in the incident x-ray beam to diffract a particular energy, and a second crystal of the same lattice spacing that is moved to intercept the diffracted beam and re-diffract so that it is parallel to the original x-ray beam. This allows a wide energy range of monochromatic x-rays to be selected and end up in the same position on the sample.

The principle characteristics of a monochromator that are important for XAFS are *the energy resolution*, and the reproducibility and stability of the monochromator. Energy resolutions of $\sim 1\,\mathrm{eV}$ at 10 keV are readily achieved with silicon monochromators, and sufficient for XAFS. Stability and reproducibility of the monochromator is sometimes challenging, as the angular precisions of monochromators needed for XAFS are typically on the order of 10^{-4} degrees so that a very small change in Bragg angle corresponds to a noticeable energy shift. In addition, small temperature drifts of the monochromator can cause noticeable drifts on the energy. For the most part, these features are generally set by the beam-line and are generally not a problem at modern beam-lines designed for XAFS measurements.

Despite their name, monochromators based on Bragg diffraction do not select only one energy (or color) of light, but also *harmonics* (integer multiplies) of that energy. These higher energies will not far above the absorption edge, and so not be absorbed efficiently by the sample. This can cause many subtle problems with the data that are hard to diagnose, including significant *glitches* and noise in the data. There are two

main strategies for removing harmonics. The first is to slightly misalign or "de-tune" the two crystals of the monochromator. This will reduce the transmitted intensity of the higher-energy harmonics much more than it reduces the intensity of the principle energy. De-tuning in this way can be done dynamically, often by putting a small piezo-electric crystal on the second monochromator crystal to allow fine motions to slightly misalign the two crystals. The second method for removing harmonics is to put an x-ray mirror in the beamline so that it reflects the principle energy much more efficiently than the higher energy harmonics. Ideally, both of these strategies can be used, but it is generally necessary to use at least one of these approaches.

Getting linear detectors to measure I_0 and I for transmission measurements is not especially difficult. A simple ion chamber (a parallel plate capacitor filled with an inert gas, and with a high voltage across it through which the x-ray beam passes) is generally more than adequate, as these detectors themselves are generally very linear over a wide range of x-ray intensities. The currents generated from the detectors are quite low (often in the picoampere range, and rarely above a microampere) and need to be amplified and transmitted to a counter. Noise in transmission lines and linearity of the amplification systems used for ion chambers (and other detectors) can cause signal degradation. Typical current amplifiers can have substantial non-linearities at low and high ends of their amplification range, and so have a range of linearity limited to a few decades. For this reason, significant dark currents are often set and one must be careful to check for saturation. For fluorescence measurements, several kinds of detectors can be used in addition to ion chambers, and linearity can become an important issue and depend on details of the detector.

With a good source of monochromatic x-rays and a good detection system, accurate and precise transmission measurements on uniform samples of appropriate thickness, are generally easy. These do require some care to make sure the beam is well-aligned on the sample, and that the sample is homogeneous and free from pinholes. Achieving a noise level of 10^{-3} for fluorescence measurements is certainly possible but can be somewhat more challenging, especially for very low concentration samples.

For concentrated samples (that is, samples in which the element of interest is a major component), XAFS should be measured in transmission. To do this, we need enough transmission through the sample to get a decent signal for I. With, $t = \log(I/I_0)$, we typically adjust the sample thickness t so that $\mu t \approx 2.5$ above the absorption edge and/or the edge step $\Delta\mu(E)t \approx 1$. For Fe metal, this gives $t = 7\,\mu\text{m}$, while for many solid metal-oxides, t is often tens of microns. For dilute solutions, sample thickness are typically in the millimeter range.

In addition to requiring the right thickness for transmission measurements, the sample must be uniform, and free of pinholes. For a powder, the grain size cannot be much bigger than an absorption length. If these conditions can be met (which can be challenging at times) a transmission measurement is very easy to perform and gives excellent data. This method is usually appropriate for model compounds, and elements with concentrations $> 10\%$.

For thick samples or lower concentrations (down to the ppm level and occasionally lower), monitoring the x-ray fluorescence is the preferred technique. In a fluorescence XAFS measurement, the x-rays emitted from the sample will include the fluorescence
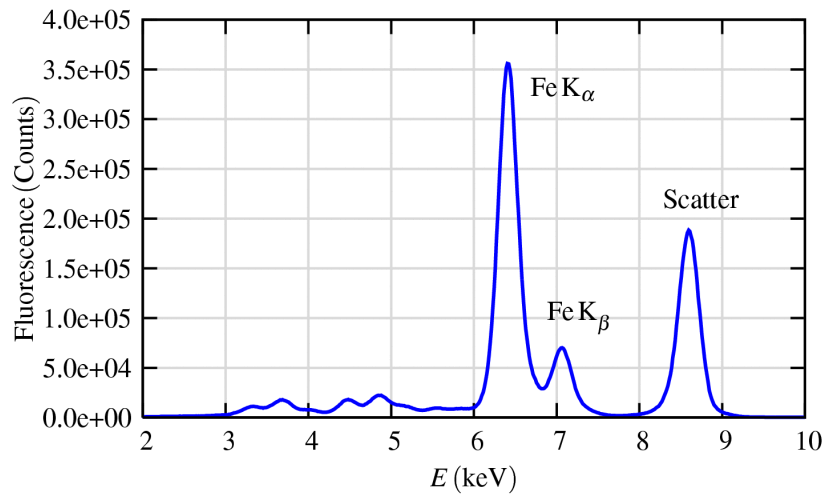
Figure 4.1: X-ray fluorescence spectra from an Fe-rich mineral (an olivine), showing the Fe K_{α} and K_{β} emission lines, and the elastically (and nearly-elastically) scattered peaks. At lower energies, Ca, Ti, and V peaks can be seen.

line of interest, fluorescence lines from other elements in the sample, and both elastically and inelastically (Compton) scattered x-rays. A typical fluorescence spectra is shown in Fig 4.1, which shows Fe K_{α} and K_{β} fluorescence lines along with the elastically scattered peak (unresolvable from the Compton scatter), as well as fluorescence lines from Ca, Ti, and V. In many cases the scatter or other fluorescence lines will dominate the fluorescence spectra.

There are two main considerations for making good fluorescence XAFS measurements: the solid angle collected by the detector and the energy resolution for fluorescence lines. The need for solid angle is easy to understand. The fluorescence is emitted isotropically, and we'd like to collect as much of the available signal as possible. X-rays that are elastically and inelastically (for example, Compton) scattered from the sample are not emitted isotropically because the x-rays from a synchrotron are *polarized* in the plane of the synchrotron, (a fact we've neglected up to this point). The polarization means that elastic scatter is greatly suppressed at $90°$ to the incident beam, in the horizontal plane. Therefore, fluorescence detectors are normally placed at a right angle to the incident beam.

Energy resolution for a fluorescence detector can be important as it allows discrimination of signals based on energy, so that scattered x-rays and fluorescence lines from other elements can be suppressed relative to the intensity of the fluorescence lines of interest is collected. This lowers the background intensity, and increase the signal-to-noise level. Energy discrimination can be accomplished either physically, by filtering out unwanted emission before it gets to the detector, or electronically after it is detected.

An example of a commonly used physical filter is to place a Mn-rich material between an Fe-bearing sample and the fluorescence detector. Due to the Mn K absorp-
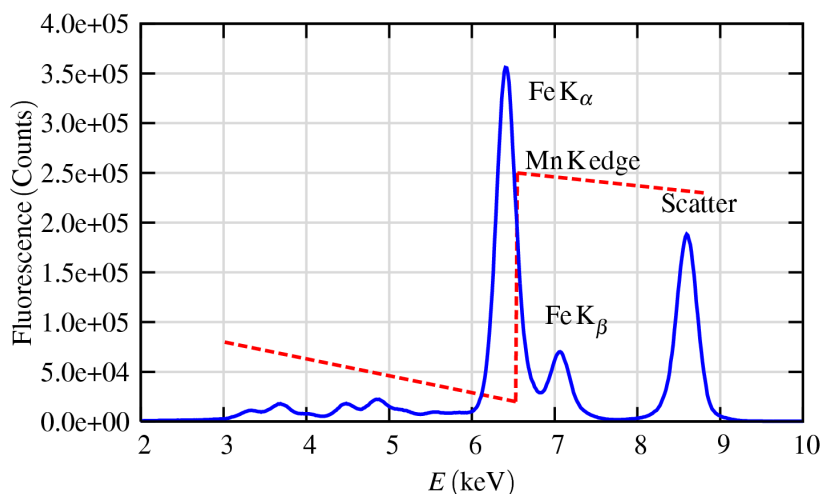
Figure 4.2: The effect of a "Z-1" filter on a measured fluorescence spectra. A filter of Mn placed between sample and detector will absorb most of the scatter peak, while transmitting most of the Fe K_α emission. For samples dominated by the scatter peak, such a filter can dramatically improve the signal-to-noise level.

tion edge, Mn will preferentially absorb the scatter peak and pass the Fe K_α line (see Fig 4.2). A simple filter like this can be used with a detector without any intrinsic energy resolution, such as an ion chamber. To avoid re-radiation from the filter itself, a set of slits (Soller slits) is often used to preferentially collect emission from the sample and block the emission from the filter, as shown in Fig 4.3. Such and arrangement can be very effective especially when the signal is dominated by scatter, and when the concentrations are in the range of hundreds of ppm and greater.

Energy discrimination can also be done electronically on the measured x-ray emission spectra after it has been collected in the detector. A common example of this approach uses a solid-state Si or Ge detector, which can achieve energy resolutions of a $\sim 200\,\text{eV}$ or better, and are typically run with resolutions better than $1\,\text{keV}$. The spectrum shown in Fig 4.1 was collected with such a Ge solid-state detector. These detectors have an impressive advantage of being able to measure the full x-ray fluorescence spectra, which is useful in its own right for being able to identify and quantify the concentrations of other elements in the sample. Because unwanted portions of the fluorescence spectra can be completely rejects, these detectors can be used for XAFS measurements with concentrations down to ppm levels. Though solid-state detectors have many advantages, they have a few drawbacks:

Dead time: the electronic energy discrimination takes a finite amount of time, which limits the total amount of signal that can be processed. These detectors typically saturate at $\sim 10^5\,\text{Hz}$ of *total* count rate or so. When these rates are exceeded, the detector is effectively unable to count all the fluorescence, and is said to be "dead" for some fraction of the time. It is common to use ten (or more!) such detectors
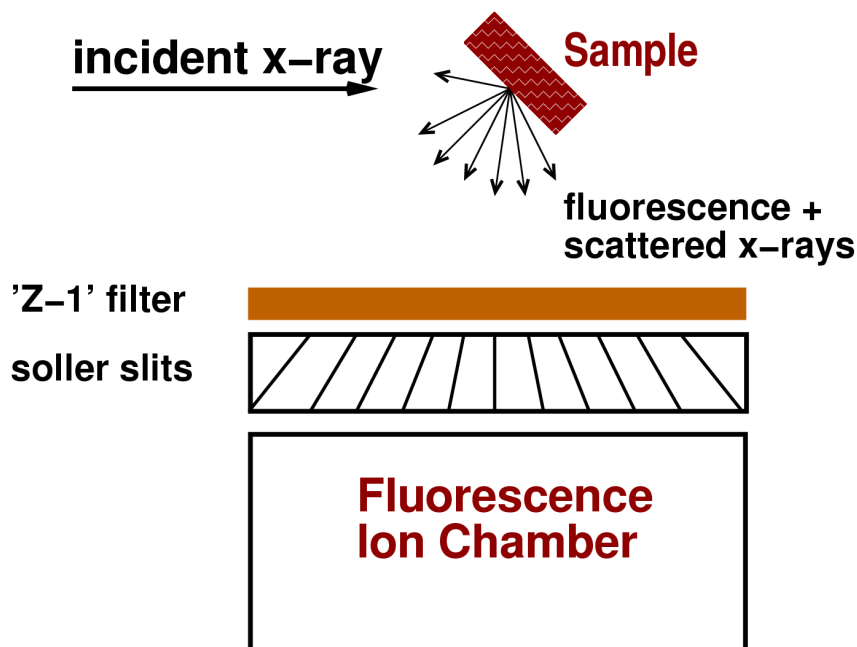
incident x-ray **Sample**

**fluorescence +
scattered x-rays**

'Z-1' filter

soller slits

**Fluorescence
Ion Chamber**

Figure 4.3: The practical use of "Z-1" filter for energy discrimination of a flu-
orescence spectra. The filter placed between sample and detector will absorb
most of the scatter peak. But it can itself re-radiate. Since the filter's emis-
sion will also be isotropic, a set of metal Soller slits pointing at the sample will
preferentially absorb the emission from the filter.

in parallel. Even then, the limit of total intensity incident on these detectors can
limit the quality of the measured XAFS.

Complicated: Maintaining, setting up, and using one of these is much more work
than using an ion chamber. The detectors usually must be kept at liquid nitrogen
temperatures, and the electronics for energy discrimination have a wide-range of
"ease-of-use". The detectors and electronics are also fairly expensive.

Despite these drawbacks the use of solid-state detectors is now fairly common prac-
tice for XAFS, especially for dilute and heterogeneous samples, and the detectors and
electronics themselves are continually being improved.

Before we leave this section on x-ray fluorescence measurements, there is one more
important effect to discuss: *self-absorption*. The term can be somewhat confusing.
Certainly, the sample itself can absorb many of the fluoresced x-rays. For example
for a dilute low-Z element (say, S) in a dense, high-Z matrix (say, Pb oxide), the S
fluorescence will be severely attenuated and the measured signal will be dictated by the
escape depth of the fluoresced x-ray.

Though an important consideration, this is not what is usually meant by *self-absorption*.
Rather, the term self-absorption usually refers to the case where the penetration depth
into the sample is dominated by the element of interest. In the worst case for self-

absorption (a thick sample of a pure element), the XAFS simply changes the penetration depth into the sample, but essentially all the x-rays are absorbed by the element of interest. The escape depth for the fluoresced x-ray is generally much longer than the penetration depth, so that essentially all absorbed x-rays cause a fluoresced x-ray. This severely dampens the XAFS oscillations. For very concentrated samples, there may be no XAFS oscillations at all!
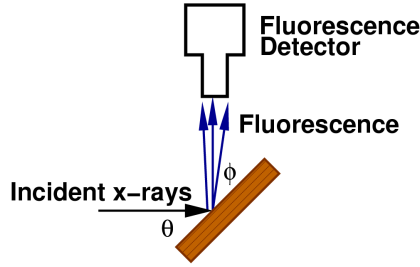
Earlier we said that for XAFS measured in fluorescence

$$\mu(E) \propto I_f/I_0. \tag{4.1}$$

This is a slight oversimplification. The probability of fluorescence *is* proportional to the absorption probability but the fluorescence intensity that we measure has to travel back through the sample to get to the detector. Since all matter attenuates x-rays, the fluorescence intensity, and therefore the XAFS oscillations, can be damped due to this self-absorption effect. More correctly, the measured fluorescence intensity goes as (see Fig. 4.4)

Figure 4.4: fluorescence x-ray absorption measurements, showing incident angle θ and exit angle ϕ.

$$I_f = I_0 \frac{\epsilon \Delta\Omega}{4\pi} \frac{\mu_\chi(E)\left\{1 - e^{-[\mu_{\text{tot}}(E)/\sin\theta + \mu_{\text{tot}}(E_f)/\sin\phi]t}\right\}}{\mu_{\text{tot}}(E)/\sin\theta + \mu_{\text{tot}}(E_f)/\sin\phi} \tag{4.2}$$

where ϵ is the fluorescence efficiency, $\Delta\Omega$ is the solid angle of the detector, E_f is the energy of the fluorescent x-ray, θ is the incident angle (between incident x-ray and sample surface), ϕ is the exit angle (between fluoresced x-ray and sample surface), $\mu_\chi(E)$ is the absorption from the element of interest, and $\mu_{\text{tot}}(E)$ is the *total* absorption in the sample,

$$\mu_{\text{tot}}(E) = \mu_\chi(E) + \mu_{\text{other}}(E) \tag{4.3}$$

Eq. 4.2 has several interesting limits that are common for real XAFS measurements. First, there is the *thin sample limit*, for which $\mu t \ll 1$. The $1 - e^{-\mu t}$ term then becomes $\approx [\mu_{\text{tot}}(E)/\sin\theta + \mu_{\text{tot}}(E_f)/\sin\phi]\,t$ (by a Taylor series expansion), which cancels the denominator, so that

$$I_f \approx I_0 \frac{\epsilon \Delta\Omega}{4\pi} \mu_\chi(E)t \tag{4.4}$$

Alternatively, there is the *thick, dilute sample limit*, for which $\mu t \gg 1$ and $\mu_\chi \ll \mu_{\text{other}}$. Now the exponential term goes to 0, so that

$$I_f = I_0 \frac{\epsilon \Delta\Omega}{4\pi} \frac{\mu_\chi(E)}{\mu_{\text{tot}}(E)/\sin\theta + \mu_{\text{tot}}(E_f)/\sin\phi}. \tag{4.5}$$

We can then ignore the energy dependence of μ_{tot}, leaving

$$I_f \sim I_0 \mu_\chi(E) \tag{4.6}$$

These two limits (very thin or thick, dilute samples) are the best cases for fluorescence measurements.

For relatively thick, concentrated samples, for which $\mu_\chi \sim \mu_{\text{other}}$, so that $\mu_\chi \sim \mu_{\text{tot}}$ we cannot ignore the energy dependence of μ_{tot}, and must correct for the oscillations in $\mu_{\text{tot}}(E)$ in Eq. 4.2. As said above, for very concentrated samples, $\mu_{\text{tot}}(E) \approx \mu_\chi(E)$, and the XAFS can be completely lost. On the other hand, if the self-absorption is not too severe, it can be corrected using the above equations.

Finally, these self-absorption effects can be reduced for thick, concentrated samples by rotating the sample so that it is nearly normal to the incident beam. With $\phi \to 0$ or the *grazing exit limit*, $\mu_{\text{tot}}(E_f)/\sin\phi \gg \mu_{\text{tot}}(E)/\sin\theta$, giving

$$I_f \approx I_0 \frac{\epsilon \Delta\Omega}{4\pi} \frac{\mu_\chi(E)}{\mu_{\text{tot}}(E_f)/\sin\phi} \tag{4.7}$$

which gets rid of the energy dependence of the denominator.

In certain situations, monitoring the intensity of emitted electrons (which includes both Auger electrons and lower-energy secondary electrons) can be used to measure the XAFS. The escape depth for electrons from material is generally much less than a micron, making these measurements more surface-sensitive than x-ray fluorescence measurements. These electron yield measurements are generally most appropriate for samples that are metallic or semiconductor (that is, electrically conducting enough so that the emitted electrons can be replenished and the sample not become charged). For these reasons, measuring the XAFS in electron yield is not very common, and details of these measurements will be left for further reading.

Chapter 5

XAFS Data Reduction

No matter whether $\mu(E)$ is measured in transmission or fluorescence (or electron emission), the data reduction and analysis are essentially the same. First the raw data is reduced to and then. After that, can be analyzed using the XAFS equation. In this section, we'll outline the steps of data reduction:

1. Convert measured intensities to $\mu(E)$, possibly correcting systematic measurement errors such as self-absorption effects and detector dead-time.

2. Subtract a smooth pre-edge function from $\mu(E)$ to get rid of any instrumental background and absorption from other edges.

3. Identify the threshold energy E_0, typically as the energy of the maximum derivative of $\mu(E)$.

4. Normalize $\mu(E)$ to go from 0 to 1, so that it represents the absorption of 1 x-ray. The normalized spectra are useful for XANES analysis.

5. Remove a smooth post-edge background function to approximate $\mu_0(E)$.

6. Isolate the XAFS $\chi(k)$, where $k = \sqrt{2m(E - E_0)/\hbar^2}$.

7. k-weight the XAFS $\chi(k)$ and Fourier transform into R-space

These steps are best shown graphically, in Figures 5.1, 5.2, 5.3, 5.4, and 5.5. Throughout these figures, transmission XAFS data from FeO is shown.

By far the most "confusing" and error-prone step in XAFS data reduction is the determination and removal of the post-edge background spline function that approximates. This is somewhat unfortunate, as it does not need to be especially difficult. The main point to keep in mind is that the function should not remove the XAFS itself, and needs to remove only the very low frequency components of.

The Fourier transform is critical to XAFS analysis, and a few important points should be made about it. The first thing to notice from Fig 5.5 is that two peaks are clearly visible – these correspond to the FeO and Fe-Fe distances in FeO. Thus the Fourier transformed XAFS can be used to isolate and identify different coordination
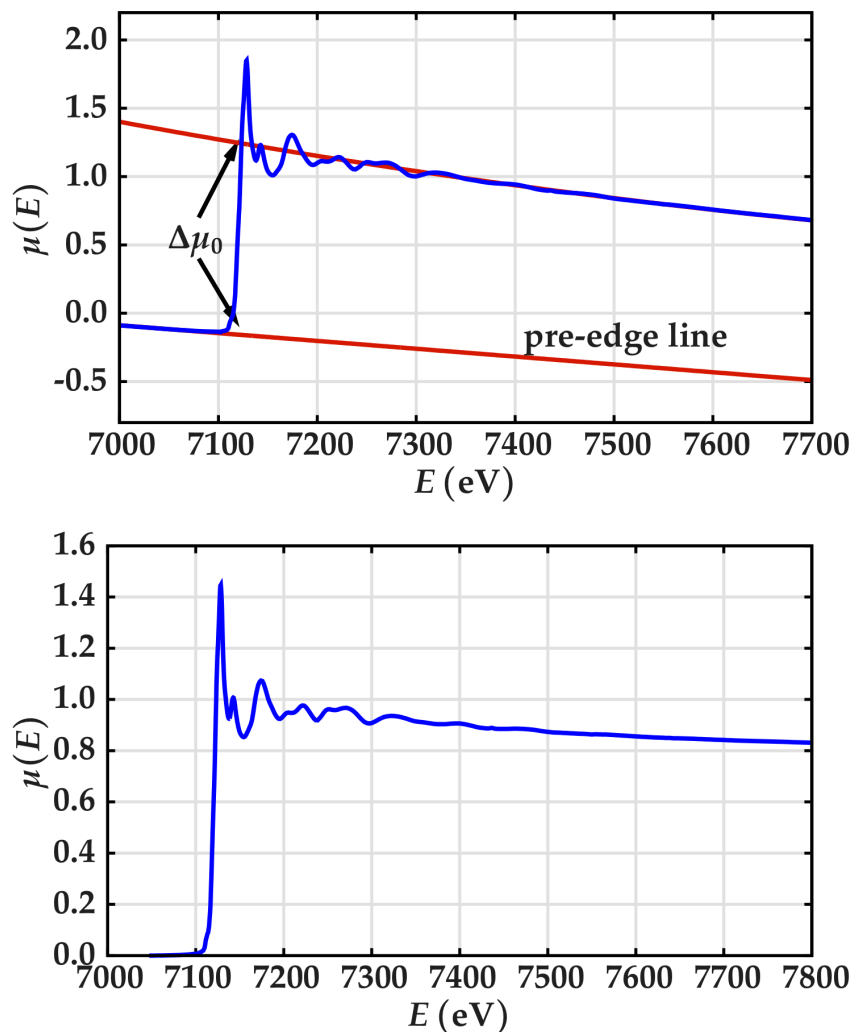
Figure 5.1: XAFS pre-edge subtraction and normalization (top). First, a pre-edge line (or simple polynomial) is fitted to the spectrum below the edge. The jump in the edge is approximated, and the spectrum is normalized by this value. The resulting normalized spectrum is shown in the bottom panel.

spheres around the absorbing Fe atom. The next thing to notice is that the first peak occurs at 1.6 Å, while the FeO distance in FeO is more like 2.14 Å. This is not an error, but is due to the scattering phase-shift – recall that the EXAFS goes as $\sin[2kR + \delta]$. This phase-shift is typically 0.5 Å or so.

The Fourier Transform is a complex function. It is common to display only the magnitude of as shown on the left of Fig 5.5. When we get to modeling the XAFS using, it will be important to keep in mind that has both real and imaginary components.
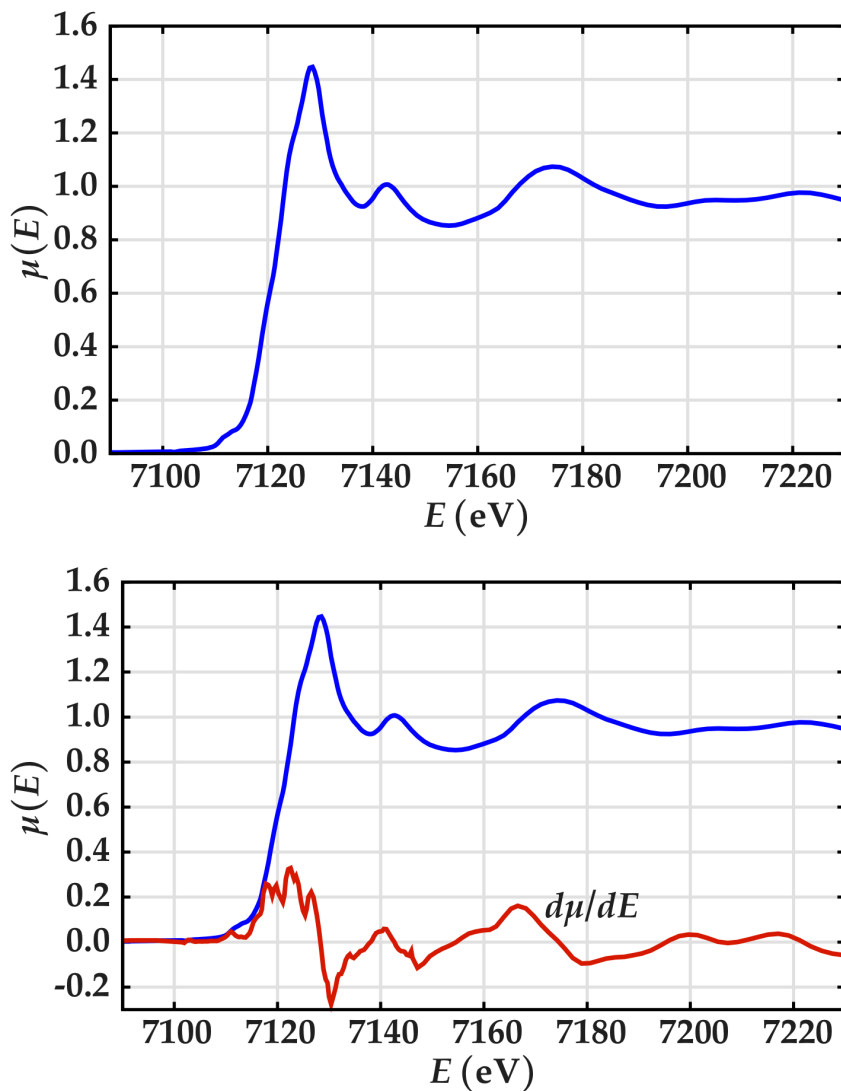
Figure 5.2: The XANES portion of the XAFS spectrum (top), and the identification of from the maximum of the derivative in (left). This selection of is somewhat arbitrary, so we'll keep this in mind when doing the XAFS refinement later.
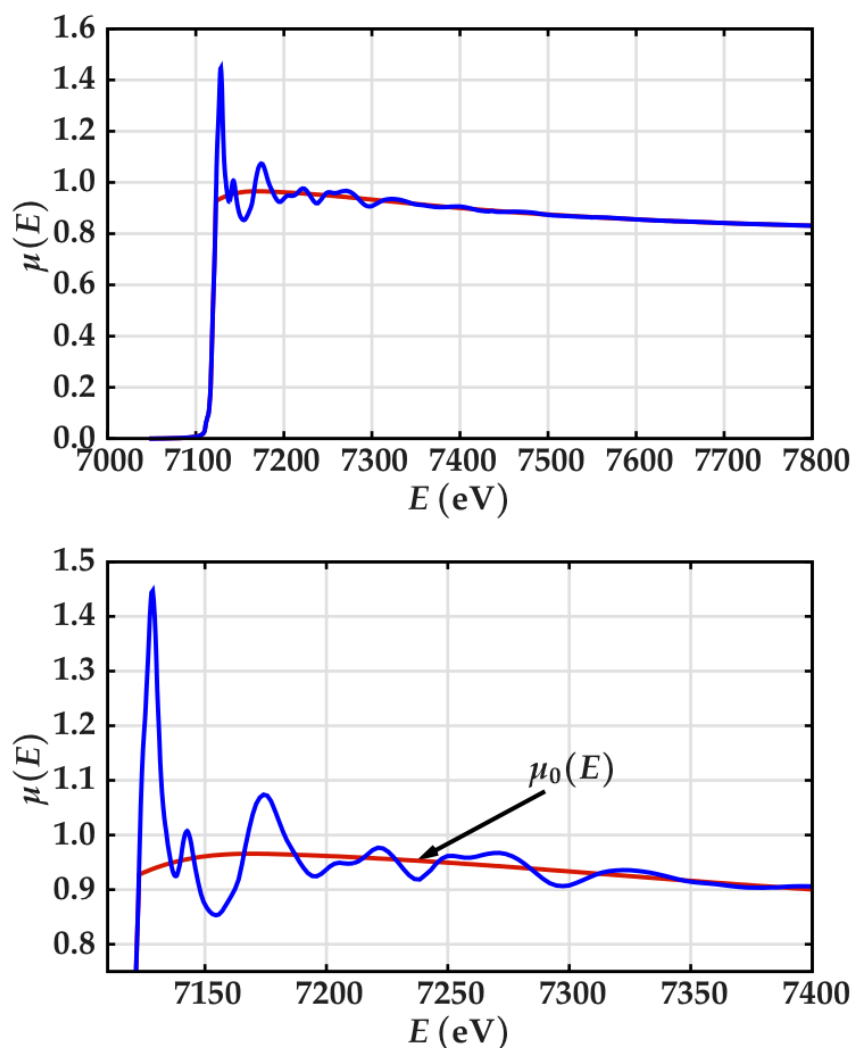
Figure 5.3: Post-edge background subtraction of XAFS. Since we don't have a measurement of $\mu_0(E)$, the absorption from an isolated atom, we approximate this with a smooth spline. This can be somewhat dangerous, as a flexible spline could match the whole $\mu(E)$! We want a spline that matches only the low frequency components of $\mu(E)$.
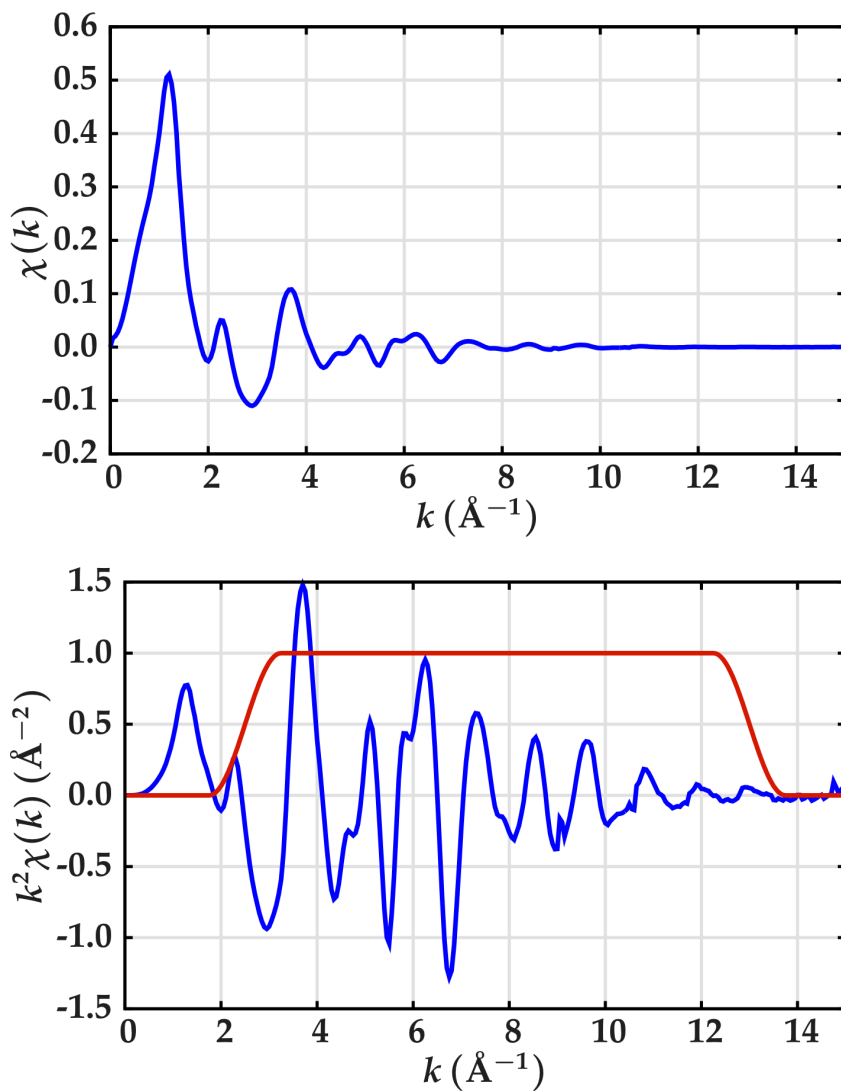
Figure 5.4: The EXAFS $\chi(k)$ (top) decays quickly with. Weighting by k^2 (bottom) amplifies the oscillations at high k. Also shown on the bottom panel is a Window Function we'll multiply $k^2\chi(k)$ by before doing a Fourier transform.
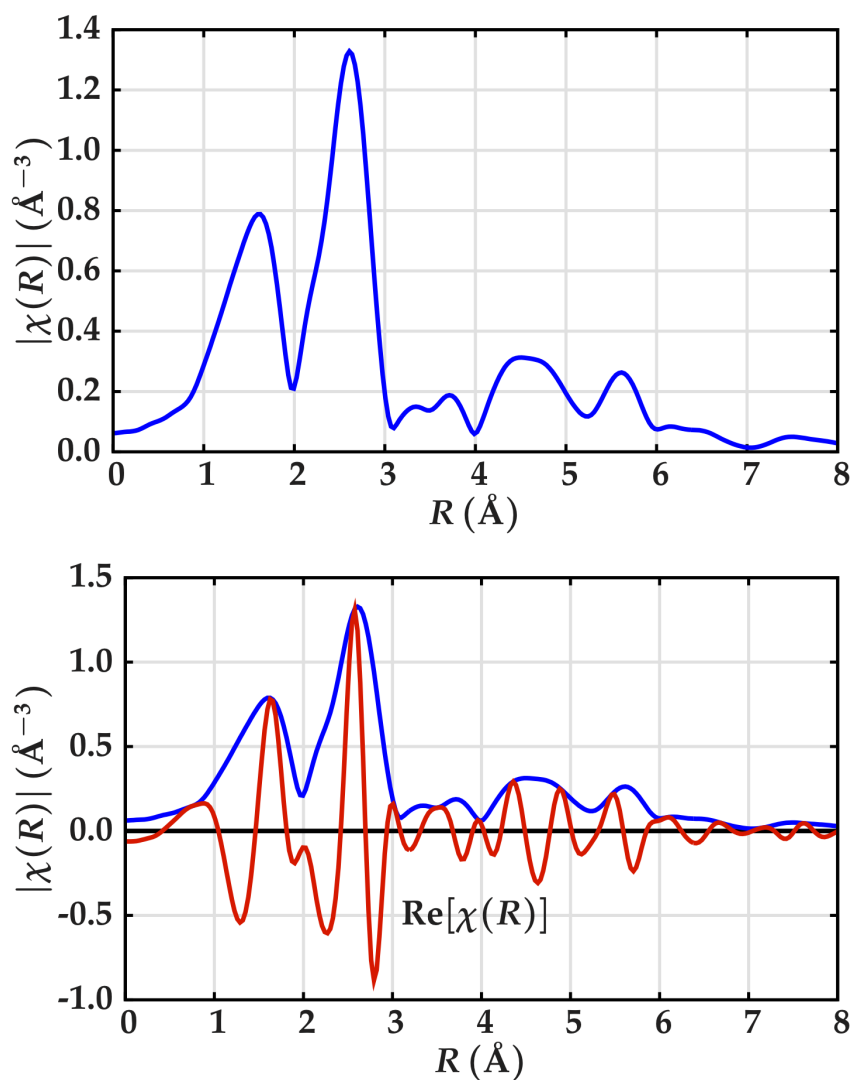
Figure 5.5: The Fourier Transformed XAFS, $\chi(R)$. On the top, the magnitude $|\chi(R)|$ is shown – this is the most common way to view the data. But the Fourier transformed XAFS is a complex function, with both real and imaginary parts. The bottom panel shows the Real part of $\chi(R)$ as well as $|\chi(R)|$.

Chapter 6

XAFS Data Modeling

In this section, we'll work through an example of structural refinement of EXAFS. The FeO data shown in the previous section will be analyzed here. Of course, we know the expected results for this system, but it will serve to demonstrate the principles of XAFS modeling. FeO has a simple rock salt structure, with Fe surrounded by 6 O, with octahedral symmetry.

Starting with this structure, we can calculate the scattering amplitude and phase-shifts and theoretically. The complete calculation is beyond the scope of this treatment, but don't worry to much by that phrase "we'll calculate these theoretically"! These functions are actually fairly easy to calculate using one of a few different computer programs – for the calculations here, the FEFF program was used. The results of the FEFF calculation are stored in simple files containing the scattering factors and mean-free-path for a given coordination shell. The calculations in these files can be used directly in a number of analysis programs.

Once we have these theoretical scattering factors, we can use them in the EXAFS equation to refine structural parameters from our data. That is, we'll use the calculated functions $f(k)$ and $\delta(k)$ (and also $\lambda(k)$) in the EXAFS equation to predict the and modify the structural parameters R, N, and σ^2 and also allow E_0 to change until we get the best-fit to the $\chi(k)$ of the data. Because of the availability of the Fourier transform, we actually have a choice of doing the refinement with the measured $\chi(k)$ or with the Fourier transformed data. Because working in R-space allows us to selectively ignore higher coordination shells, using R-space for the fitting has several advantages and we will use it in the examples here. When analyzing the data this way, the full complex XAFS $\chi(R)$, not just the magnitude $|\chi(R)|$, must be used.

A typical fit to the first FeO shell of FeO done in this way is shown in Fig 6.1. The result from this fit gives an FeO distance of $R = 2.10 \pm 0.02$ Å, an O coordination number of $N = 5.8 \pm 1.8$, a mean-square disorder of $\sigma^2 = 0.015 \pm 0.005\,\text{Å}^2$, and a shift in E_0 of $--3.1 \pm 2.5\,\text{eV}$.

It is instructive to look at this "best-fit" in k-space, as shown in Fig 6.2. From this and Fig 6.1, it is evident that the higher frequency components (i.e., the second shell of Fe-Fe) dominate. This is a useful reminder of the power of the Fourier transform in XAFS analysis – it allows us to concentrate on one shell at a time and ignore the others.

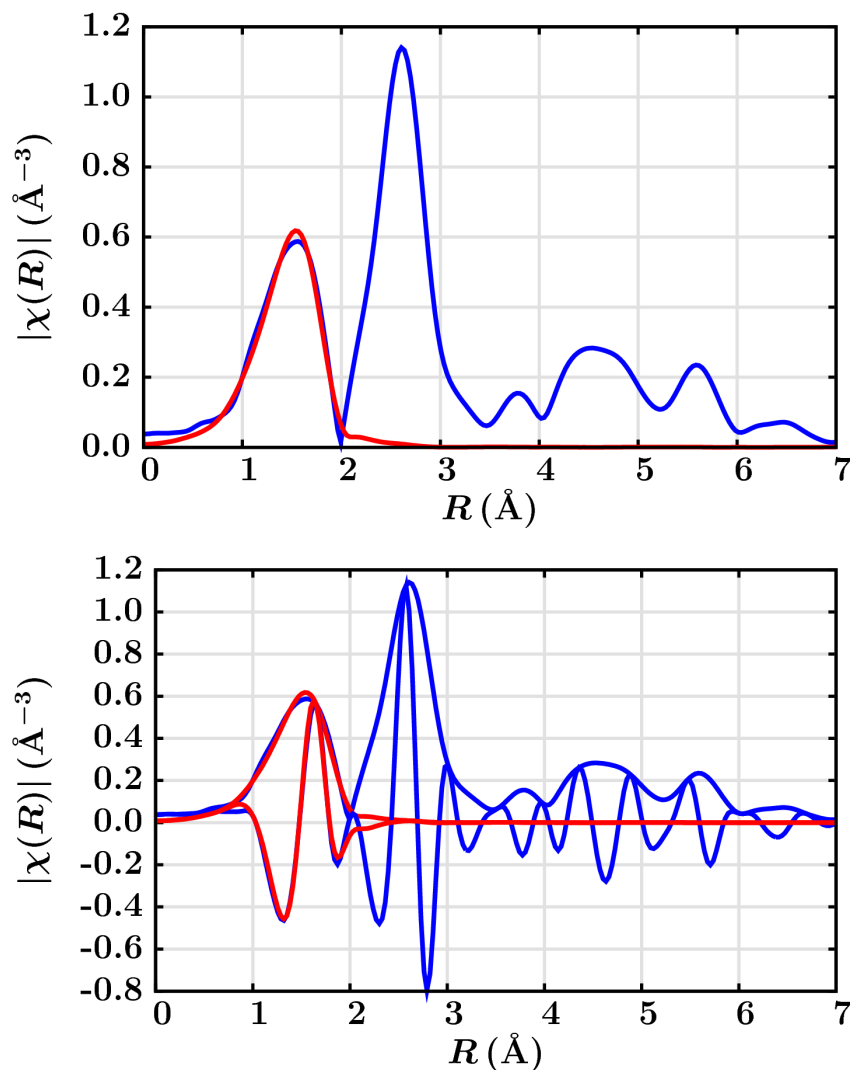We can include the second shell in the model simply by adding another shell to the

Figure 6.1: First shell fit to the EXAFS of FeO. On the top, the $|\chi(R)|$ of the data and best-fit are shown, while the real parts of $|\chi(R)|$ for both the data and best fit are also shown in the bottom panel.

XAFS sum and using calculated scattering factors for Fe-Fe scattering. We will now refine the R, N, and σ^2 for the Fe-Fe shell as well as the FeO shell, and also refine a single value of E_0.

At this point, we should discuss the number of free variables allowed in the refinement and the amount of "independent measurements" that can be extracted from the data. Standard signal analysis tells us that the maximum number of free variables that can be effectively fit in a refinement depends on the k and R-range considered. It turns out that the maximum number of parameters that can be determined from an XAFS spectra is about $N_{max} \, \Delta k \, \Delta R \, \pi$, for k-range Δk and R-range ΔR. The "about" should be stressed here – this number is an estimate, and probably an upper estimate! For the
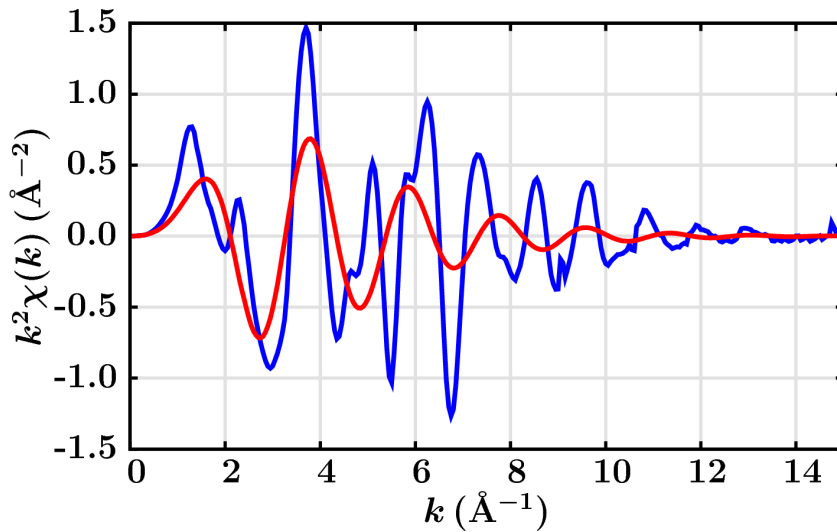
Figure 6.2: EXAFS $\chi(k)$ data and best-fit to the first shell of FeO. It is clear that higher-frequency (that is, higher R) components contribute to this spectrum.

analysis of the first two shells of FeO, we'll use the data from $k = 2.5$ to $12.5\,\text{Å}^{-1}$ and R=1.0 to 3.0 Å in the refinement, which gives $N_{\text{max}} = 12.7$. We'll use 7 variables, safely below this limit.

The fit results for this refinement gives an FeO distance of $R = 2.10 \pm 0.02$ Å, an O coordination number of $N = 6.0 \pm 1.0$, and a means-square disorder of $\sigma^2 = 0.015 \pm 0.003\,\text{Å}^2$. For Fe-Fe, the distance refines to $R = 3.05 \pm 0.02$ Å, with a coordination number of $N = 11.7 \pm 1.3$, and a mean-square disorder of $\sigma^2 = 0.014 \pm 0.002\,\text{Å}^2$. The best-fit value for E_0 is found to be -2.1 ± 0.8 eV. The structural values for distances and coordination number are very consistent with the known crystal structure of FeO. The fits are shown in Fig 6.3, and individual contributions to the total best-fit spectrum are shown in both k- and R-space in Fig 6.4.

While we've seen that structural refinement of XAFS data can be fairly straightforward, real analysis can be much more complex, with either mixed coordination shells or effects from *multiple-scattering*, in which the photo-electron scatters from 2 or more atoms before returning to the absorbing atom. These cases can be accommodated, and more sophisticated fitting models can be applied to the refinement, but these topics are beyond the scope of this discussion.
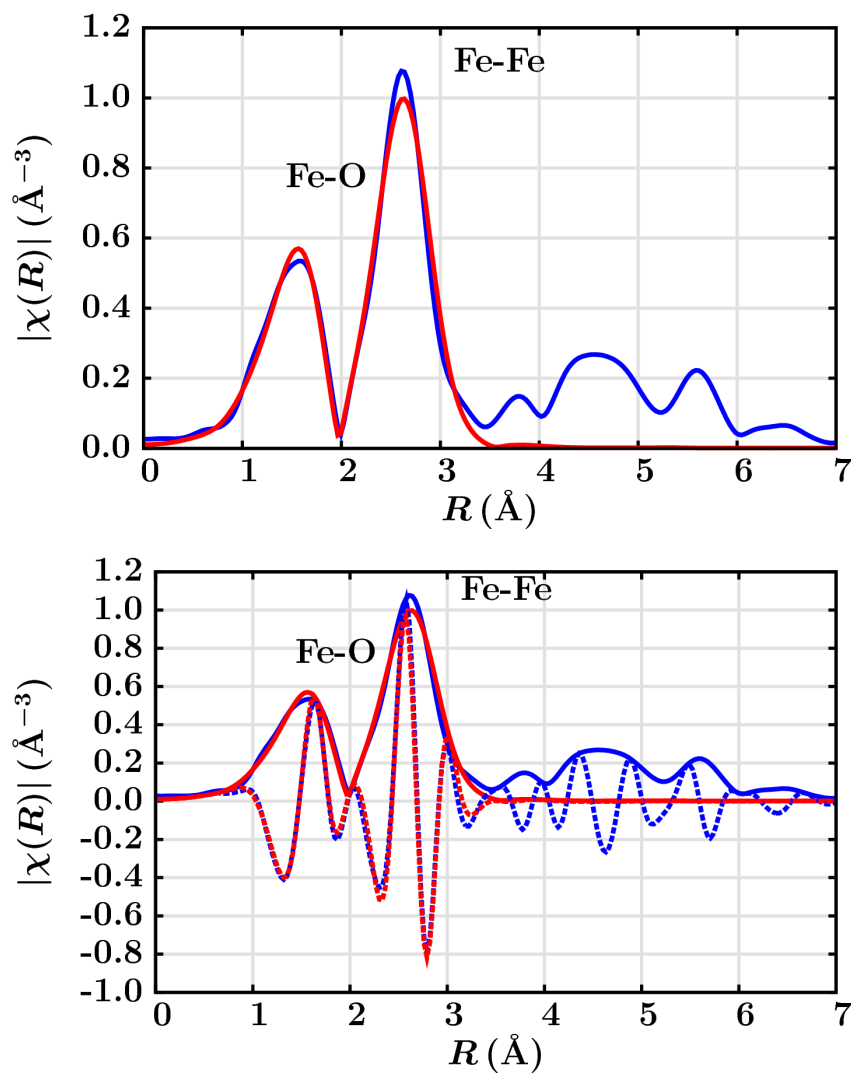
Figure 6.3: First and second shell fit to the EXAFS of FeO. On the top, the $|\chi(R)|$ of the data and best-fit are shown, while the real parts of $|\chi(R)|$ for both the data and best fit are also shown in the bottom panel.
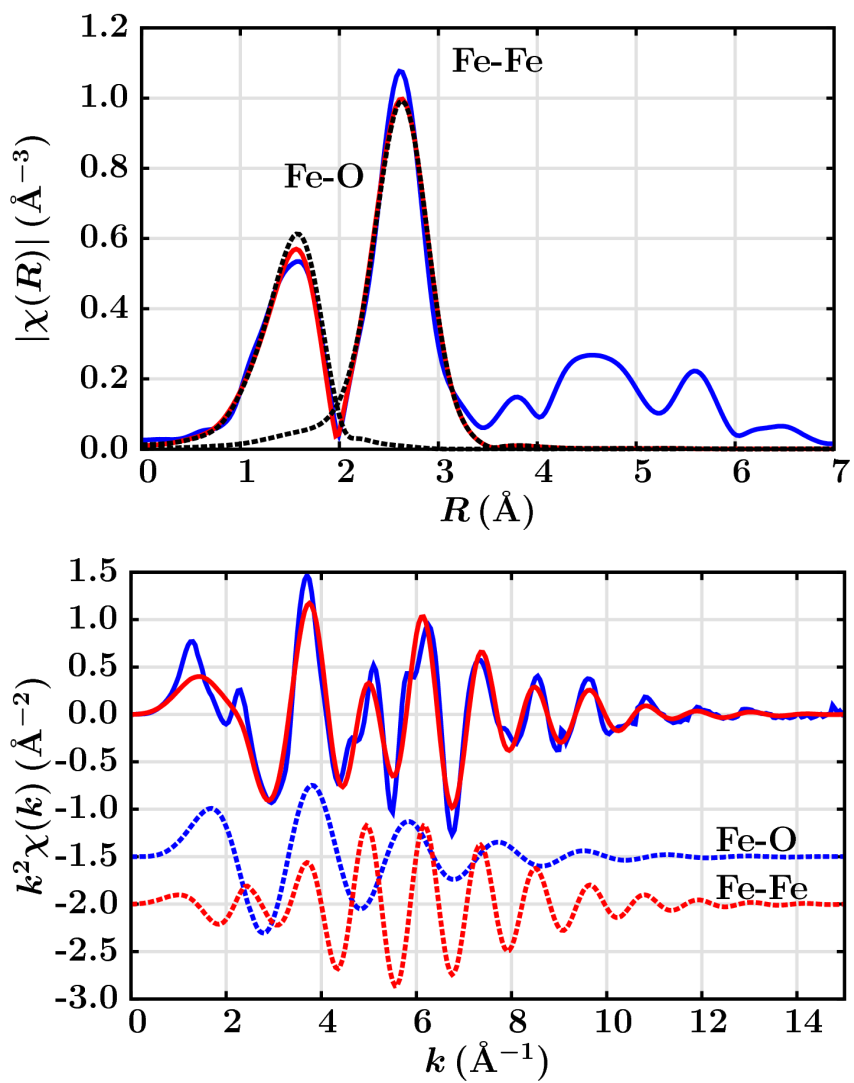
Figure 6.4: The individual contributions of FeO and Fe-Fe for the EXAFS of FeO. On the top, the contributions are shown in R-space, while on the bottom panel they are shown in k-space.

Chapter 7

XANES Interpretation

Finally, we return to the XANES portion of the spectrum. Since XANES is a much larger signal than EXAFS, XANES can be done at lower concentrations, and at less-than-perfect sample conditions. The interpretation of XANES is complicated by the fact that there is not a simple analytic (or even physical) description of XANES. The main difficulty is that the EXAFS equation breaks down at low-k, due to the $1/k$ term and the increase in the mean-free-path at very low-k. Still, there is much chemical information from the XANES region, notably formal valence (very difficult to experimentally determine in a nondestructive way) and coordination environment. Fig 7.1 shows the XANES spectra for several iron compounds. Clearly, the edge position and shape is sensitive to formal valence state, ligand type, and coordination environment. If nothing else, XANES can be used as a fingerprint to identify phases.

Even though there is not a useful "XANES Equation", we can go back to the picture of section 3, and especially the concept of available state for the photo-electron. For K shell absorption, where the core-level is a $1s$ state, the photo-electron has to end up in a p state (in general, the photo-electric effect changes the orbital quantum number l to $l \pm 1$). Thus, even if there are available states with the right energy, there might be no $1s$ absorption if there are no available p states. For EXAFS, where the energies are well-above the threshold energy, this is rarely an important concern. For XANES, on the other hand, this can play a very important role. Transition metal oxides, for example, usually have many unfilled $3d$ electrons near the Fermi level, and a filled $3p$ band. There are empty $2p$ electron states from the oxygen, but these are too far away to appreciably over-lap with the metal $1s$ band. Therefore, the metal $3d$ electrons do not normally participate in the absorption process unless there is a strong hybridization of the O $2p$ and metal $3d$ levels. The XANES spectra are then especially sensitive to such hybridization – a topic we'll return to when discussing XANES.

The situation can be even more dramatic – as Fig 7.2 shows for Cr^{3+} and Cr^{6+} oxides. For ions with unfilled d-electrons bands, the pd hybridization is dramatically altered depending on the coordination environment, which much stronger hybridization for tetrahedral coordination than for octahedral coordination. Since the photo-electron created due to a 1s core level (a K-shell) must have p-like symmetry, the amount of overlap with the d-electron orbitals near the Fermi level can dramatically alter the number of available states to the p-electron, causing significant changes in the XANES
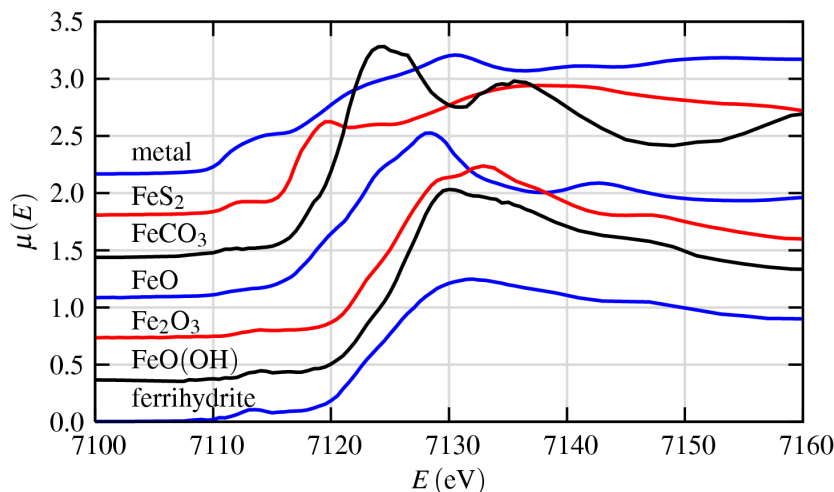
Figure 7.1: Fe K-edge XANES of Fe metal and several Fe compounds.

spectrum. For the case of Cr^{6+} pd hybridization results in a highly localized molecular orbital state, giving a well-defined peak below the main absorption edge, indicating a transition to a bound electronic state.

Though the lack of a simple analytic expression complicates XANES interpretation, XANES can be described qualitatively (and nearly quantitatively) in terms of

Coordination chemistry: regular, distorted octahedral, tetrahedral coordination, as for Cr.

Molecular orbitals: $p - d$ orbital hybridization, crystal-field theory, and so on.

Band-structure: the density of available electronic states.

Multiple-scattering: multiple bounces of the photo-electron.

These chemical and physical interpretations are all related, of course. As discussed in the introduction, it all boils down to determining which electronic states the photo-electron can fill.

An important and common application of XANES is to use the shift of the edge position to determine the valence state. Fig 7.3 shows the valence dependence of Fe metal and oxides of Fe^{2+} and Fe^{3+} (and a mixture of these two). With good model spectra, Fe^{3+}/Fe^{2+} ratios can be determined with very good precision and reliability. Similar ratios can be made for many other ions. The heights and positions of pre-edge peaks can also be reliably used to empirically determine oxidation states and coordination chemistry. These approaches of assigning formal valence state based on edge features and as a fingerprinting technique make XANES somewhat easier to crudely interpret than EXAFS, even if a complete physical understanding of all spectral features is not available.
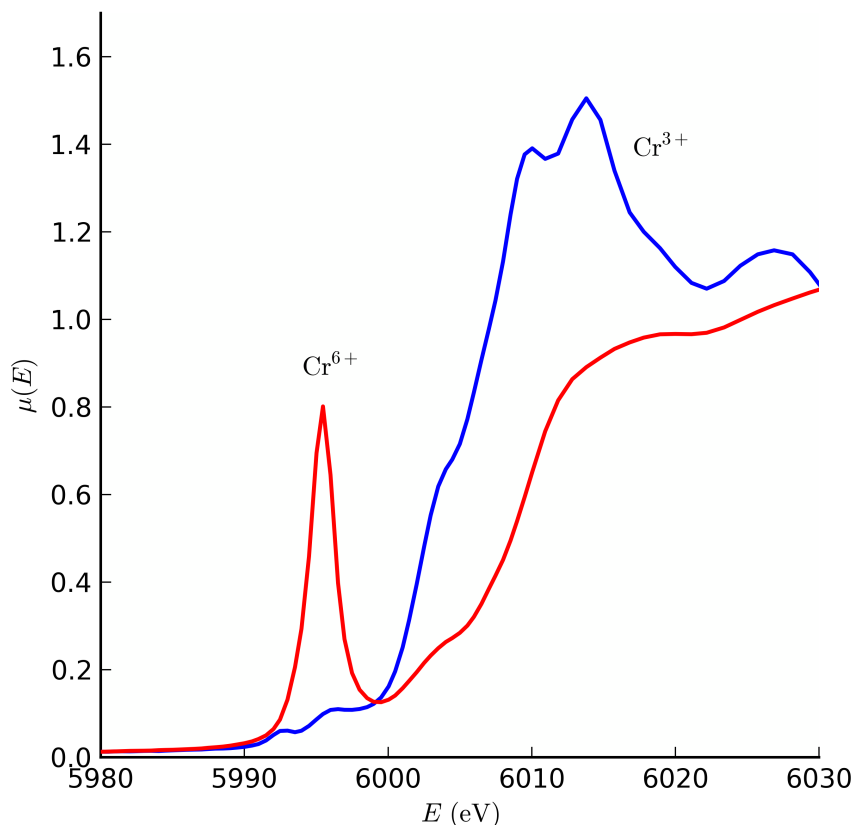
Figure 7.2: Cr K-edge XANES for Cr^{3+} and Cr^{6+} oxides. Here the strong pre-edge peak in the Cr^{6+} spectrum is a consequence of the tetrahedral symmetry causing considerable overdue of the empty d-electron orbitals with the p-states that the photo-electron must fill.

For many systems, XANES analysis based on linear combinations of known spectra from "model compounds" is sufficient to tell ratios of valence states and/or phases. More sophisticated linear algebra techniques such as Principle Component Analysis and Factor Analysis can (and are) also be applied to XANES spectra.

XANES is considerably harder to fully interpret than EXAFS. Precise and accurate calculations of all spectral features are still difficult, time-consuming, and not always reliable. This situation is improving, but at this point, quantitative analyses of XANES using *ab initio* calculations are very rare. Still, such calculations can help explain which bonding orbitals and/or structural characteristics give rise to certain spectral features, but are beyond the scope of this treatment, and will have to wait for another day.
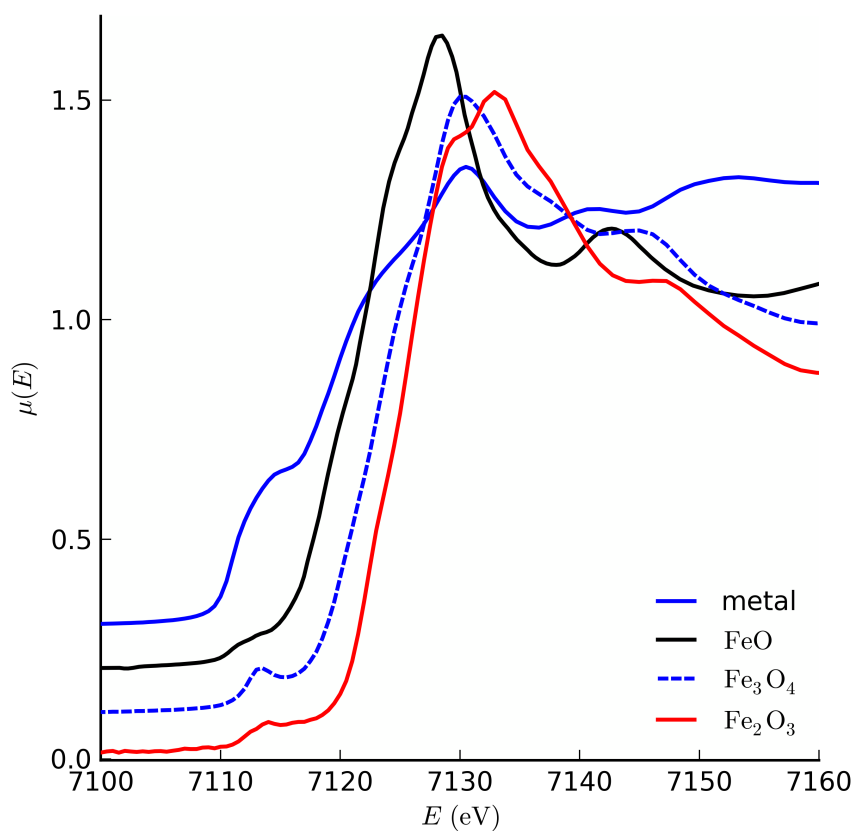
Figure 7.3: Fe K-edge XANES of Fe metal and several Fe oxides, showing a clear relationship between edge position and formal valence state. In addition, the shapes, positions, and intensities of pre-edge peaks can often be correlated to oxidation state.

Bibliography

[1] Xray Absorption: Principles, Applications, Techniques of EXAFS, SEXAFS, and XANES, in Chemical Analysis 92, D. C. Koningsberger and R. Prins, ed., John Wiley & Sons, 1988.

[2] Principles and Applications of EXAFS, Chapter 10 in Handbook of Synchrotron Radiation, pp 995–1014. E. A. Stern and S. M. Heald, E. E. Koch, ed., North-Holland, 1983.

[3] Elements of Modern X-ray Physics, J. Als-Nielsen and D. McMorrow John Wiley & Sons, 2001.